HHS Public Access

Author manuscript

Cell Calcium. Author manuscript; available in PMC 2020 March 01.

Published in final edited form as:

Cell Calcium. 2019 March ; 78: 1–14. doi:10.1016/j.ceca.2018.12.006.

Regulation of Ca^{2+} Signaling by Acute Hypoxia and Acidosis in Cardiomyocytes derived from Human Induced Pluripotent Stem Cells

José-Carlos Fernández-Morales[1], **Wei Hua**[1], **Yuyu Yao**[1], and **Martin Morad**[1,2]

[1]Cardiac Signaling Center of MUSC, USC and Clemson, Charleston, South Carolina.

[2]Department of Pharmacology, Georgetown University Medical Center, Washington, DC, USA

Abstract

Aims: The effects of acute (100s) hypoxia and/or acidosis on Ca^{2+} signaling parameters of human induced pluripotent stem cell-derived cardiomyocytes (hiPSC-CM) are explored here for the first time.

Methods and Results: 1) hiPSC-CMs express two cell populations: *rapidly-inactivating* I_{Ca} myocytes (τ_i<40ms, in 4–5 day cultures) and *slowly-inactivating* I_{Ca} ($\tau_i \geq$ 40ms, in 6–8 day cultures). **2)** Hypoxia suppressed I_{Ca} by 10–20% in rapidly- and 40–55% in slowly-inactivating I_{Ca} cells. **3)** Isoproterenol enhanced I_{Ca} in hiPSC-CMs, but either enhanced or did not alter the hypoxic suppression. **4)** Hypoxia had no differential suppressive effects in the two cell-types when Ba^{2+} was the charge carrier through the calcium channels, implicating Ca^{2+}-dependent inactivation in O_2 sensing. **5)** Acidosis suppressed I_{Ca} by ~35% and ~25% in rapidly and slowly inactivating I_{Ca} cells, respectively. **6)** Hypoxia and acidosis suppressive effects on Ca-transients depended on whether global or RyR2-microdomain were measured: with acidosis suppression was ~25% in global and ~37% in RyR2 Ca^{2+}-microdomains in either cell type, whereas with hypoxia suppression was ~20% and ~25% respectively in global and RyR2-microdomaine in rapidly and ~35% and ~45% respectively in global and RyR2-microdomaine in slowly-inactivating cells.

Conclusions: Variability in I_{Ca} inactivation kinetics rather than cellular ancestry seems to underlie the action potential morphology differences generally attributed to mixed atrial and ventricular cell populations in hiPSC-CMs cultures. The differential hypoxic regulation of Ca^{2+}-signaling in the two-cell types arises from differential Ca^{2+}-dependent inactivation of the Ca^{2+}-channel caused by proximity of Ca^{2+}-release stores to the Ca^{2+} channels.

Corresponding author: Professor Martin Morad, Cardiac Signaling Center, USC, MUSC & Clemson University, Charleston, SC. 29425, Phone number: +1(843) 792-3898, Fax number: +1(843) 792-0664, moradm@musc.edu.

AUTHOR CONTRIBUTIONS

Designed the experiments: M. Morad.

Conducted experiments and analysis: Jose-Carlos Fernandez-Morales, Wei Hua, Yuyu Yao.

Wrote the manuscript: Jose-Carlos Fernandez-Morales, and M. Morad.

DECLARATION OF INTEREST STATEMENT

No conflicts of interest, financial or otherwise, are declared by the author(s).

Keywords

L-type Ca(2+) channel; hypoxia; acidosis; ischemia; human induced Pluripotent Stem Cells derived cardiomyocytes

INTRODUCTION

Ischemic heart disease and acute myocardial infarction are leading causes of death from cardiovascular pathology in developing countries [1]. Myocardial infarction often triggers arrhythmia when the human heart is subjected to acute hypoxia during coronary occlusion or when oxygen demands of the heart exceeds its work load [2]. The development of cardiomyocytes derived from human induced pluripotent stem cells (hiPSC-CMs), not only is a promising strategy for patient-specific cell therapy [3, 4], but also allows *in vitro* experimental approach to study the mechanisms underlying cardiac pathology in human tissue [5]. Recent reports suggest that hiPSC-CMs are a good *in vitro* electrophysiological model of human cardiomyocytes because: 1) similar to mature mammalian cardiomyocytes, hiPSC-CMs express robust levels of L-type Ca^{2+} channels and Ca^{2+}-induced Ca^{2+} release (CICR), critical for EC-coupling [6–9]; 2) regulation of the L-type Ca^{2+} channels and calcium signaling by Ca^{2+}, phosphorylation, and pharmacological agents in hiPSC-CMs mimics closely that of mammalian cardiomyocytes [10, 11]. Encouraged by possible human-relevance of these reports, we probed the pathophysiological effects of hypoxia and ischemia in hiPSC-CMs[12]. Although there are a few reports on the effects of chronic hypoxia in hiPSC-CMs [13–16], there are no reports on the effects of acute hypoxia and acidosis on calcium signaling of hiPSC-CMs. Since L-type cardiac Ca^{2+} channels have been implicated in oxygen-sensing of the rat heart [17] through a mechanism involving the interaction of heme-oxygenase with CaM/CaMKII domain of L-type Ca^{2+} channel [18], it was critical to determine whether similar mechanism are also at play in human stem cell-derived cardiomyocytes thus obviating possible subtle species differences in the hypoxic responses and its adrenergic regulation between adult and neonatal rat cardiomyocytes [19] and human heart.

Here we explored the effects of acute hypoxia and acidosis on human iPS-derived cardiomyocytes and found that the susceptibility to hypoxia and acidosis was partly dependent on the inactivation kinetics of L-type Ca^{2+} channels. Generally, two groups of cells were consistently identified: those with rapidly inactivating I_{Ca}, time constant ~ 10ms and those with slowly inactivating I_{Ca}, tau ~40ms. Our data suggests that the older slowly inactivating I_{Ca} cells were more sensitive to hypoxia but not to acidosis as compared to younger rapidly inactivating I_{Ca} cells.

METHODS

Cell culture of human pluripotent stem cells and cardiac differentiation

Human pluripotent stem cells (hiPSC-K3) obtained from Stephen Duncan at Medical University of South Carolina [20] were routinely cultured in E8 medium (Life Technologies/GIBCO) on Matrigel (BD Biosciences) coated tissue culture plates with daily media change

at 37 °C with 5% (vol/vol) CO_2. Differentiation was performed following the protocols of Xiaojun Lian *et al* [21]. Briefly, dissociated hiPSCs were plated in 12 well plates with matrigel and then treated with 12 μM CHIR 99021, a GSK3β inhibitor for 24 h in RPMI/B-27 without insulin. 72 h after CHIR99021 treatment, 5 mM IWP2, a *wnt* processing inhibitor, was added to culture with the same media for 48 h. After 48 h of continued culture in RPMI/B-27 without insulin, the cells were maintained in RPMI/B-27 medium with insulin for the rest of the time.

hiPSC-CMs dissociation

The hiPSC-CM cell lines were grown in culture for 30–40 days before dissociating and re-plating for electrophysiological and Ca^{2+} imaging experiments. The mechanical dissociation of hiPSC-CM clusters into single cardiomyocytes has been made following the next protocol: 1) Visualize spontaneously beating EBs under the microscope, and mechanically dissect them from the gelatin coated wells with a curved 23G needle. 2) Aspirate the dissected EBs with their original medium using pipette and transfer them to a 50 ml test tube. 3) Centrifuge the EBs suspension within the test tube at a rate of 1000 rpm for 5 min. 4) Re-suspend the EBs in 10 ml of fresh medium and transfer them to a 15 ml test tube. 5) Centrifuge at a rate of 900 rpm for 2 min. 6) Wash the cells 3×with PBS (centrifuge between washings at a rate of 900 rpm for 2 min). 7) Add 5 ml of 1 mg/ml collagenase type IV solution (5mg collagenase IV-low Ca^{2+} solution) to the centrifuged washed cells. 8.) Incubate the solution with EBs in 37°C bath for 5 min. 9) Incubate with rotator for additional 45 min in 37°C. 10) Centrifuge at a rate of 1000 rpm for 5 min. 11) Re-suspend cells with 3ml of re-suspension solution. Incubate in 37°C for additional 15 min. 12) Centrifuge at a rate of 1000 rpm for 5 min. The single hiPSC-CMs then were plated on fibronectin (2.5 μg/ml)-coated glass coverslips in 6 well plates after collagenase B treatment, and then incubated for 36–72 h before their use in electrophysiological or Ca^{2+} imaging experiments.

Electrophysiological recordings

Whole-cell Ca^{2+} currents (I_{Ca}) was recorded using the perforated-patch mode of the patch-clamp technique [22, 23], induced by amphotericin B (1mg/ml) [24, 25]. After waiting approximately 5–10 minutes, series resistance fell below 20 MΩ and tight seals (>1 GΩ) were achieved using an intracellular solution composed (in mM): 145 Glutamic Acid, 9 NaCl, 1 $MgCl_2$ and 10 HEPES, pH 7.2~7.3, adjust with CsOH. Cells were bathed in a Tyrode's solution composed of (in mM): 137 NaCl, 1 $MgCl_2$, 2 $CaCl_2$ or 2 $BaCl_2$ (depending on the experimental protocol), 5.3 KCl, 10 glucose, and 10 HEPES. The duration of different experimental treatments (Normoxia/Hypoxia and/or pH 7.4/pH 6.7, with or without ISO in all the figures of the manuscript was always 100s, except for the washing of ISO in normoxia condition, lasting often ~ 200s. In all experiments I_{Ca} was recorded at room temperature (22–25 °C) using a Dagan voltage-clamp amplifier controlled by pClamp-9 software running on a personal computer. Borosilicate patch pipettes with 5–7 MΩ resistance were prepared the previous hour using a horizontal pipette puller (Model P-87, Sutter Instruments, CA). The series resistance was monitored until it decreased to < 20 MΩ, after which the experiments were began. The liquid junction potential was corrected before seal formation. In all recordings, the holding potential was set at −40 mV in order to

inactivate Na^+ channels. I_{Ca} or I_{Ba} were activated by100-ms depolarizing voltage pulses to 0 mV. I_{Ca} or I_{Ba} were measured at 5 s intervals except when electrophysiological measurements were combined with fluorescence measurements, in which case they were measured 25s intervals. The measured currents were filtered at 1 or 10 kHz, digitized at 10 or 100 kHz, and plotted and analyzed in terms of magnitude and time constants of their inactivation, using Graph Prism (GraphPad Corp., San Diego, CA, USA) and pCLAMP 9.0 software. Membrane potential (Em) oscillations were registered using the current-clamp configuration of the patch-clamp technique. The holding potential was set at −50 mV in voltage clamp mode, and the series resistance continuously monitored until it had decreased to < 20 MΩ. After this the amplifier was shifted to the current-clamp mode, (with no current "injection" applied). Only cells with leak currents of < 5 pA were used for experimental analysis. Cell size was estimated from membrane capacitance measurements, a method commonly utilized to obtain an estimate of the plasma membrane area of the cells, providing an indirect indicator of the cell size. This approach is particularly useful in hiPSC-CMs which have few membrane invaginations or t-tubular system at these stages of development [26, 27]. Note that earlier studies have shown a positive linear correlations between membrane capacitance and cell volume in cardiomyocytes of several species [28].

To study the effects of hypoxia on ionic currents, single voltage-clamped hiPSC-CMs were perfused with external Tyrode's solutions equilibrated with atmospheric O_2 (normoxic) or 100% N_2 (hypoxic). We bubbled hypoxic solutions for at least 1h to make sure that nitrogen displaces all the oxygen molecules from our reservoirs and then we began the rapid application of the hypoxia solution by the perfusion pipette placed in close proximity of the cell. Solution exchange took place within 50 ms using an electronically controlled perfusion system equipped with five barrels loaded with normoxic and hypoxic Tyrode's solutions containing varying electrolyte concentrations and pharmacological agents desired for the different type of experiments [29]. The O_2 pressure was measured with a needle probe which registered < 5 mmHg for the hypoxic solutions both in the bubbled reservoirs and near the port for solution outflow into the main chamber. HEPES (10 mM) was used to buffer the extracellular solutions, which prevented changes in the pH of the external solutions with bubbling of N_2. Acidification of the media to pH 6.7 was achieved by addition of isotonic HCl. The pH of all solutions was carefully determined using a pH meter at room temperature (~ 25°C).

Fluorometric Ca^{2+} measurements in voltage-clamped cells

Single isolated beating hiPSC-CMs were subjected to 100 ms depolarizing voltage-clamp pulses (−40 to 0 mV) that activated I_{Ca} triggering intracellular Ca^{2+} transients. Intracellular global Ca^{2+} signals were measured with the fluorescent Ca^{2+}- indicator dye Fluo-4AM (2 μM, Invitrogen), after 40 min of incubation of cells at 37 °C and 5% CO_2. The fluorescence probe and dye were excited at 460 nm using a LED-based illuminator (Prismatix, Modiin Ilite, Israel) and gated aperture and Ca^{2+}-dependent fluorescent light (>500nm) was detected with a photomultiplier tube using a Zeiss Axiovert 100 TV inverted microscope.

Focal RyR2 Ca^{2+} micro-domains were measured using genetically engineered virally introduced biosensors GCaMP6-FKBP targeted to FKBP-12.6 (calstabin-2) binding site of

RyR2 (K_d=250 nM, λ_{ex}=488 nm). The probe uses calmodulin as Ca^{2+} chelator and green fluorescent protein (GFP) as reporting fluorophor, which allows it to sense the Ca^{2+} in the micro-domains of dyadic clefts where CICR takes place. For the probe and the fluorescent Ca^{2+}- indicator dye the parameters of the Ca^{2+} signals analyzed were the basal fluorescence (F_0) and the peak of the Ca^{2+} transient (ΔF).

Chemical products

Chemical compounds to make saline solutions, as well as isoprenaline hydrochloride were purchased from Sigma (Sigma-Aldrich, St Louise, MO, USA). Amphotericin B was acquired from Fisher Scientific (Pittsburgh, PA, USA). Every experimental day, a stock solution of isoprenaline hydrochloride was prepared in deionized water and amphotericin B in DMSO. The inhibitors CHIR 99021 were acquired from Selleckchem (Houston, TX, USA) and IWP2 from TOCRIS (Minneapolis, MN, USA), E8, RPMI and B-27 culture mediums were purchased from Life Technologies/GIBCO (Grand Island, NY, USA). The novel and potent $Ca_V1.3$-highly selective antagonist, 1-(3-chlorophenethyl)-3-cyclopentylpyrimidine-2,4,6-(1*H*,3*H*,5*H*)-trione [30], was purchased from Calbiochem-EMD chemicals (San Diego, CA, USA).

Statistical analysis

Data are presented as scatter grams, showing the individual data points of each cell together with the mean (represented in blue line) ± standard error of the mean (SEM, represented by the red error lines). The number of cells and cultures are indicated in parentheses (*n*, *N*). Paired or unpaired two-tailed Student's *t* test was used to compare means according to the dependent or independent between the data set to compare. A *P* value equal or smaller than 0.05 was selected as the limit of significance. Significance levels were indicated with an increasing number of asterisks ($*P < 0.05$, $**P < 0.01$, $***P < 0.001$) and when not being significant by (n.s., $P > 0.05$). Data sets were tested for normality (Kolmogorov-Smirnov normality test), an assumption for the application of the Student's t-test. We found that some groups didn't fit well to normal distributions, a nonparametric statistical test was used (Mann-Whitney's rank sum test to compare two samples). In other cases, one-way ANOVA with post-hoc multiple comparisons was used to establish if there were significant differences between the means of 3 or more independent groups, not related to each other. Scatter plot were used to explore the association between cell size, the suppression of the I_{Ca} by hypoxia and the tau inactivation of the I_{Ca}. The correlations between these variables were analyzed by Pearson linear correlation coefficient. To analyze I_{Ca} decay or *tau inactivation* of the I_{Ca} (τ_i), single exponential fits were applied to the decaying part of individual I_{Ca} traces using a simplex optimization algorithm as follows: $y = y_0 + \{1 - [A_i \exp(- t / \tau_i)]\}$ where A_i represent the amplitudes of the I_{Ca} and τ_i represent the time constants of inactivation respectively. To study the tail currents triggered by calcium channel deactivation, the tail current time course of rapidly and slowly inactivating I_{Ca} cells were fitted by a bi-exponential equation with a fast (τ_1) and slow (τ_2) time constants. The bi-exponential fitting produces similar correlation coefficient average that using mono-exponential fitting (0.968 vs. 0.988) and precision ($1e^{-4}$ for both cases). We also analyzed the peak amplitude of the I_{Ca} tail for both cell types. All statistical analysis was performed

using GraphPad Prism 7.0 (GraphPad Software, La Jolla, CA) and MS Excel (Microsoft, Redmond, WA).

RESULTS

I: Two different cell populations of hiPSC-CMs cultures based on Ca^{2+} channel inactivation kinetics.

Pharmacological, biophysical and molecular characterization.—Calcium currents were measured in hiPSC-CMs in 4 to 8 day cultures using the perforated-patch mode of the whole-cell patch-clamp technique, (day zero was the day of the mechanical dissociation of hiPSC-CM clusters into single cardiomyocytes). Unexpectedly, we found two distinct populations of hiPSC-CMs based on the inactivation kinetics of their I_{Ca} (Fig. 1A and B). In one group of cells, I_{Ca} inactivated rapidly (τ_i = 21.40 ± 1.16 ms, n=48 cells), while in another set I_{Ca} inactivated slowly (τ_i = 51.95 ± 1.01 ms, n=56 cells). The latter group of cells were more abundant in older 6 to 8 day cultures (Fig. 1C, F). These two cell types were found on each single day in culture, but the percentage of cells with slowly inactivating I_{Ca} was higher in older cultures while those with rapidly inactivating I_{Ca} decreased from 48.3 % at day 4 to 10.0% at day 8 of culture, Fig. 1C. A positive linear correlation (r = 0.548 $p<0.0001$) was found between the cell surface area (pF) and the inactivation time constant of I_{Ca} (τ_i), Fig 1H. Smaller cells (10–30 pF) had mainly rapidly inactivating I_{Ca}, while cells larger than 30 pF had escalating slower inactivation kinetics. The dashed vertical line at τ_i = 40 ms was arbitrarily set as separation of the two cell populations (open circles, $\tau_i < 40$ ms, and those with much slower inactivating I_{Ca}, filled circles, $\tau_i \geq 40$ ms).

The distribution of the inactivation time constant (τ_i) of I_{Ca} in different days of culture could be differentiated into three main groups, based on the center of bell-shaped distributions: first group, at 4 days' culture centered at ~35 ms, second group, centered at ~55 ms at 5 and 6 days, and the third group, centered at ~85 ms at 7 and 8 days of culture (Fig. 1F). Box and colored whiskers plots (dark blue, red, green, yellow and light blue) show the distribution of the τ_i for the 4, 5, 6, 7 days of culture, with median values of 36, 50, 50, 80 and 81 ms, respectively (Fig. 1G).

Biophysical analysis: We explored the possibility of whether the calcium channels expressed in the two cell types producing I_{Ca} with rapidly or slowly inactivating kinetics represent two different calcium channels (e.g. $Ca_V1.2$ and $Ca_V1.3$) or whether the same population of channels ($Ca_V1.2$) with different modulation of their CDI is responsible for the differences in the kinetics of inactivation of the two cell types. The analysis of kinetics of tail currents generated by deactivation of I_{Ca} from 0 to −40 mVs in 60 cells fitted with two biexponential equation with a fast (τ_1) and slow (τ_2) time constants, Fig. S1, shows that the mean fast (τ_1) and slow (τ_2) time constants for the deactivation of the I_{Ca} tail were not significantly different in the two cell types (Fig. S1 C and inset traces a2 & b2), consistent with the same population of channels being responsible for the two cell types.

Molecular experiments: In support of single population idea, we found that the level of expression of $Ca_V1.2$ mRNA was markedly greater than $Ca_V1.3$ both in the early (day4) or late (day7) developmental time in culture where hiPSC-CMs with rapidly or slowly

inactivating $I_{Ca,}$ respectively, are more frequently found (Fig. S2). Consistent with mRNA studies 10 μM of a potent and selective $Ca_V1.3$ antagonist (1-(3-chlorophenethyl)-3-cyclopentylpyrimidine-2,4,6-(1*H*,3*H*,5*H*)-trione) [30], failed to block I_{Ca} in hiPSC-CMs, where 2 or 10 μM nifedipine produced ~95% block of I_{Ca} (panel D, Fig. 2).

Pharmacologically also, the data suggests that one population of channels is responsible for the two different inactivation kinetics, because we found similar nifedipine sensitivity even in the presence of low concentrations of this dihydropyridine [31] and the same dose response relation for the rapidly and slowly inactivating I_{Ca} (Fig. 2). These finding, therefore, suggest that only $Ca_V1.2$ subtype of L-type calcium channel is expressed in hiPSC-CMs but its CDI is differentially modulated during cell growth and development.

Cell size, estimated from membrane capacitance measurements increased significantly with culture age, reflecting cell growth, ranging from 27.50 ± 3.19 pF at day 4, to 31.61 ± 2.01 pF at day 5, to 45.69 ± 3.22 pF at day 6, to 50.97 ± 4.73 pF at day 7 and 69.98 ± 9.29 pF at day 8. Similarly, the Ca^{2+} channel current increased significantly, from 233.51 ± 30.84 pA at day 4, to 240.59 ± 20.16 pA at day 5, to 371.94 ± 53.11 pA at day 6, to 413.87 ± 52.42 pA at day 7 and finally to 552.24 ± 97.52 pA at day 8 (Fig. 1A, B, D). However, Ca^{2+} current density did not change significantly with the length of hiPSC-CMs in culture (8.49 ± 0.60 pA/pF at day 4, 7.61 ± 0.54 pA/pF at day 5, 8.14 ± 0.69 pA/pF at day 6, 8.12 ± 0.75 pA/pF at day 7 and 7.89 ± 0.73 pA/pF at day 8, Fig. 1E), suggesting that a gradual increase in the number of calcium channels occurred with the cell growth. Fig. 1I shows the differential potentiating effects of 100 nM isoproterenol (ISO) on I_{Ca} as a function of days in culture, ~85 % enhancement of I_{Ca} at day 7 as compared to day 6, and almost ~150 % enhancement at day 8 with respect to day 5 or 6.

Action potential measurements in hiPSC-CMs cultures also reflected the decay kinetics of I_{Ca}, that is, cells with shorter action potentials expressed rapidly inactivating I_{Ca} (Fig. 3B, C, H), and interestingly had a faster spontaneous pacing rate (Fig. 3A, I), while cells with longer action potential expressed slowly inactivating I_{Ca} (Fig. 3E, F, H), and had much slower spontaneous pacing rates (Fig. 3D, I). Fig 2G shows a positive linear correlation ($r = 0.75$ $p<0.0005$) between the APD_{90} (ms) and the inactivation time constant of I_{Ca} (τ_i), rapidly inactivating I_{Ca} cells (τ_i ~ 20 ms) had mainly shorter APs (APD_{90} < 800 ms) at room temperatures, while slowly inactivating I_{Ca} cells ($\tau_i \geq 40$ ms) displayed progressively longer APs ($APD_{90} \geq 800$ ms). The dashed vertical line at $\tau_i = 40$ ms was chosen to denotes approximate separation of the two cell populations (squares, $\tau_i < 40$ ms, and those with much slower inactivating I_{Ca}, triangles, $\tau_i \geq 40$ ms). Spontaneously developing APs from rapidly inactivating I_{Ca} cells also showed a significantly slower upstroke velocity (Fig. 3J). The resting membrane potential of the two cell types (data not shown) was not significantly different (~ −52 mV).

II: Hypoxia effects on cardiomyocytes derived from human induced pluripotent stem cells

A. Suppressive effect of hypoxia on I_{Ca} depends on its inactivation kinetics.

—Acute hypoxia was created by reducing PO_2 rapidly (< 1s), exchanging the normoxic solution (equilibrated with ambient air, ~21% O_2) for a hypoxic solution (bubbled with 100% N_2; PO_2 < 5 mmHg). I_{Ca} was activated with repeated depolarizations at 5 s intervals

from −40 to 0 mV, to avoid possible activation of T-type Ca^{2+} channels. Run-down was minimized by using perforated-patch mode of the patch-clamp technique, causing little or no significant decline in I_{Ca} for periods of 3 minutes in normoxic solutions (Fig. 4C and 4D, empty circles). Rapid application of hypoxic solutions produced ~5% initial reduction of I_{Ca} within the first 5 s in both cell types, continued by a gradual decrease in I_{Ca} that stabilized within the first 60 s at 16.7 ± 2.6 % (n = 8, N = 4) in cells with rapidly inactivating I_{Ca} (Fig. 4C, filled circles). In slowly inactivating I_{Ca} cells the suppression continued to increase reaching steady-state levels of 52.30 ± 9.4 % (n = 8, N = 3) in ~100 s (Fig. 4D, filled circles). In both cell types I_{Ca} recovered to its control levels in about 75 s following the return of normoxic solutions (Fig. 4C and D filled circles, see also original tracing of I_{Ca} in two representative myocytes, Fig. 4A and B).

A positive linear correlation ($r = 0.566$, $p<0.001$) was found between the degree of hypoxic suppression of I_{Ca} and the rate of its inactivation (scatter-gram and red correlation line, Fig. 4E). Despite the great variability in the hypoxic suppressive effect, the slowly inactivating population of hiPSC-CMs (the predominant cell types, Fig. 1) were highly sensitive to hypoxia (~ 50 % suppression), while hiPSC-CMs with rapidly inactivating I_{Ca} were mostly resistant (~ 15 % suppression) to acute hypoxia. Acute hypoxia also marginally, but not significantly, slowed the mean I_{Ca} inactivation time constant from the normoxic values of 16.73 ± 3.85 ms and 43.21 ± 10.29 ms, Fig. 4F.

B. Hypoxia effects on Ba^{2+} transporting calcium channels.—The suppressive effect of acute hypoxia was enhanced from 18% to 35% in adult rat cardiomyocytes when Ba^{2+} was charge carrier through the channel [17, 18]. Similarly, in rat neonatal cardiomyocytes suppression of CDI by Ba^{2+} or by increased intracellular Ca^{2+} buffering strongly enhanced the suppressive effects of hypoxia in the rapidly inactivating I_{Ca} cells [19]. Fig. 5B shows that in hiPSC-CMs too, when 2mM Ba^{2+} replaced Ca^{2+}, acute hypoxia rapidly suppressed the current within the first 5s, but in the slowly inactivating I_{Ca} cells the steady-state suppression after 100s of hypoxia was significantly smaller (39.5 % ± 2.9 %, Fig. 5B, vs. 52.30 ± 9.4 %. Fig. 4D) than in Ca^{2+} transporting channels, suggesting an additional calcium-dependent hypoxic suppressive effect. The mean inactivation time constant of I_{Ba} in hiPSC-CMs was not significantly altered by hypoxia (Fig. 5D). In this set of 10 cells, 4 of them with rapidly inactivating I_{Ca} in 2 mM Ca^{2+} (τ_i < 40 ms), increased their tau inactivation becoming slowly inactivating when the solution was replaced to normoxic Ba^{2+} solutions (Fig. 5A, $\tau_i \geq 40$ ms). Even though in some of the slowly inactivating I_{Ca} cells 2 mM Ba^{2+} failed to increase the inactivation kinetics significantly (Fig. 5A), the amplitude of the current increased from ~40% to ~100% in all 10 cells, see panel A of figure 5 (the rapidly inactivating I_{Ca} cell in 2mM Ca^{2+} with tau inactivation of 17.2 ms increased to 59.5ms in 2mM Ba^{2+}). The average suppressive effect of hypoxia in extracellular Ba^{2+} was slightly smaller, but not significantly, in the rapidly inactivating I_{Ca} cells (35.4 ± 5.7 % *vs* 41.3 ± 3.8 %), see red insert box in panel C of figure 5. These finding strongly support the assertion that the rapidly inactivating I_{Ca} is not transported by T-type channels since the inactivation kinetics and current amplitude of the low threshold T-type channel are not significantly altered by replacing Ca^{2+} with Ba^{2+} [32, 33].

Accordingly, the slow inactivation of the calcium channel, happening either innately in a population of hiPSC-CMs, or induced by transport of Ba^{2+} through the channel appeared to sensitize the channel to hypoxia, suggesting that the rapid inactivation of the calcium channel, mediated by CDI, is protective against hypoxia.

C. Regulation of the phosphorylated L-type calcium channels by hypoxia in cells with rapidly or slowly inactivating I_{Ca}.—Phosphorylation of the carboxyl tail of the α1C and β-subunits of the L-type calcium channel by PKA is known to facilitate of I_{Ca} [34, 35]. Fig. 6 shows that 100 nM isoproterenol (ISO) increased I_{Ca} by 90.21 ± 36.72 % in the cells with rapidly inactivating I_{Ca} (Fig. 6C) and by 86.48 ± 27.97 % in the cells with slowly inactivating I_{Ca} (Fig. 6D). In isoproterenol treated hiPSC-CMs hypoxia suppressed I_{Ca} by 37.57 ± 23.16 % in cells expressing the rapidly inactivating I_{Ca} (Fig. 6C) and by 51.39 ± 23.86 % in cells with slowly inactivating I_{Ca} (Fig. 6D). Note that ISO not only did not protect against hypoxia in either cell type, but in fact enhanced the effect of hypoxia on the rapidly inactivating I_{Ca} cells (37.5 ± 23.1 % suppression in ISO treated cells, Fig. 6C, *vs.* 16.7 ± 2.6 % suppression in control cells Fig. 4C, see also the effect of only hypoxia after ISO washout on the time course of the current., Fig. 6C, 11.9 ± 6.3 % I_{Ca} suppression).

The hypoxia effects were also examined on the kinetics of inactivation of I_{Ca} in phosphorylated and control cells (Fig. 6E and F). The data suggests that ISO significantly reduced τ_i in phosphorylated slowly inactivating I_{Ca} hiPSC-CMs under normoxic conditions, but had no effect under hypoxic conditions (Fig. 6B and F). A positive linear correlation ($r = 0.6394$, $p<0.001$) was found between the degree of hypoxic suppression of I_{Ca} and the rate of its inactivation (scatter-gram and red correlation line, Fig. 6E), despite the great variability in the hypoxic suppressive effect between the two cell types. Thus, we conclude that PKA-mediated phosphorylation does not protect the channel against the suppressive effects of hypoxia in hiPSC-CMs. These results are consistent with those reported in adult rat cardiomyocytes [17, 18] or in rN-CMs [19] and contrasts sharply with those described for adult guinea pig cardiomyocytes [36].

III: Effects of acidification and ischemia (Hypoxia plus Acidosis) on rapidly and slowly inactivating hiPSC-CMs.

Because episodes of ischemia result not only in tissue hypoxia, but also to acidosis due to lactic acid accumulation [37], in another set of experiments we measured the combined effects of acute acidification and hypoxia. The combined effects of hypoxia plus acidosis were studied as to approximate "*ischemia"* in our hiPS-derived CMs. After 5 s of acidosis (pH, 6.7) I_{Ca} was suppressed faster and by a greater degree in rapidly- than the slowly-inactivating I_{Ca} cells; 22.13 ± 8.63 % vs. 6.42 ± 3.17 %, Fig. 7B and F. In both cases suppression of I_{Ca} continued for ~50 seconds until steady-state levels were achieved. The final suppressive effects of acidosis were larger, but not significantly, in rapidly inactivating I_{Ca} cell-type (37.85 ± 5.95 % vs. 25.76 ± 4.83 %), Fig. 7A, E, C and G.

The suppressive effect of ischemia (100s of combined acidosis and hypoxia) on I_{Ca} were similar in magnitude in both cells types, 45.14 ± 5.42 % in rapidly inactivating I_{Ca} vs. 47.7 ± 4.28 % in slowly inactivating I_{Ca} (pink trace records of the Fig. 7A, E and panels B, C, F

and G of Fig. 7). Unexpectedly, the combined effects of acidosis and hypoxia were not additive in the slowly inactivating I_{Ca} cells as they were in rapidly inactivating hiPSC-CMs (Fig. 7C, vs. 7G).

IV: Hypoxia and Acidosis effects on global and focal Ca^{2+} Signaling in hiPSC-CMs.

The effects of acute hypoxia and acidosis on global and focal cytosolic Ca^{2+} transients were also measured using Fluo-4 AM and GCamP6-FKBP targeted to RyR2 microdomains. Ca_i-transits were triggered by 100ms depolarizing pulses followed by 1 second rapid puff of 3mM caffeine. The rise of global cytosolic Ca^{2+} by caffeine and the integration of the activated Na^+-Ca^{2+}-exchange current, I_{NCX}, [38] provided two estimates of SR calcium content. I_{Ca}, I_{NCX}, focal RyR2 μ-domain (GCaMP6-FKBP signals), the global cytosolic Ca^{2+} transients (Fluo-4 AM signals), and the diastolic $[Ca^{2+}]_i$ (baseline fluorescence, F_o) were all measured and quantified as fluorescent ratios.

a) *Global cytosolic Ca^{2+}*: The global diastolic Ca^{2+} levels of the rapidly and slowly inactivating I_{Ca} hiPSC-CMs were not significantly different (~0.3–0.4 vs ~ 0.25–0.35 arbitrary fluorescence units – AFU – respectively), and acidosis or hypoxia did not seem to alter the diastolic Ca^{2+} significantly (Fig. S3, traces C, D, I, J, and panel E and K). Global systolic $Ca^{2+}{}_i$ transients, though similar in the two cell types, were marginally higher in the slowly inactivating I_{Ca} cells (~0.10–012 vs ~0.07–0.10 AFU, Fig. S3, tracings C, D, I, J and panels F and L). Acidosis decreased the global systolic $[Ca^{2+}]_i$ slightly. There was a tendency for larger effects in the rapidly inactivating I_{Ca} cells (25.0% vs 20.2%, compare traces C & D and panel F of Fig. S3). Hypoxia, on the other hand, was more effective in suppressing the systolic $Ca^{2+}{}_i$ transients in the slowly inactivating compared to rapidly inactivating I_{Ca} cells (35.1% vs. 19.2%, traces I, J and panel L of Fig. S3), consistent with the suppressive effect of hypoxia on I_{Ca} (36.6% vs. 20.9%, tracings G, H and panel L, of Fig. S3). It is critical to note that in the latter set of experiments, cells were incubated in Fluo-4AM, which is likely to have altered the Ca^{2+} buffering capacity of the cells, and as such the effects of hypoxia and acidosis maybe dampened as compared to the set of experiments where the perforated patch clamp technique was used to monitor I_{Ca} (Fig. 4 & 7).

b) Focal Ca^{2+} transients: Diastolic Ca^{2+} levels, measured in RyR2 μ-domains using GCamP6-FKBP, were slightly but not significantly higher in rapidly inactivating I_{Ca} cells, (Fig. S4, traces C&G), and acidosis or hypoxia did not substantially modify this parameter in either cell type (Fig. S4 and S5, traces C, G and panel J). In marked contrast, however, acidosis substantially (37%) reduced the systolic GCaMP6-FKBP Ca^{2+} signals in both cell types (Fig. S4, traces C, G and panel I). I_{Ca} density was similarly suppressed by acidosis in the rapidly and slowly inactivating I_{Ca} cells (30 % vs 23 % respectively, Fig. S4, traces A, E and panel I). There was no or little difference in the Ca^{2+} content of the SR, calculated from the integral of the caffeine-induced I_{NCX} (~0.6 to 0.8 $\times$ 10^{-12} M), in the two cell types (Fig. S4 L), and was reduced similarly on exposure to 100 seconds of acidosis by 35% in both cell types (Fig. S4 B, F and L). On the other hand, hypoxia differentially suppressed the systolic GCaMP6-FKBP Ca^{2+} signals in the two cell types (25% in the rapidly vs 45% in the slowly inactivating I_{Ca} cells), panels C, G and panel I, Fig. S5. This differential effect may reflect

the differences in I_{Ca} suppressive effect of hypoxia on the slowly inactivating I_{Ca} cell type (42% vs 16 % in the rapidly inactivating I_{Ca} cells), compare panels A, E and I, of figure S5. The Ca^{2+} content of SR was also suppressed by 100 second exposure to hypoxia to a greater degree in the slowly inactivating I_{Ca} cells (50% vs 26% in rapidly inactivating I_{Ca} hiPSC-CMs), Fig. S5 B, F and L. Similar reductions in the SR Ca^{2+} store were also noted when the store content was quantified by measurements of fluorescence of GCamP6-FKBP signals (panel K, tracings D, H of Fig. S5).

DISCUSSION

Human fibroblast derived developing cardiomyocytes grown in cultures, express two cell types based on the kinetics of inactivation of their L-type Ca^{2+} channels. This finding may, in part, be responsible for the heterogeneity of action potential duration observed by many investigators working in this field and taken as evidence for the ancestral heterogeneity of hiPSC-CM cultures expressing atrial, ventricular, and conduction tissue cell-types. While the suppressive effects of hypoxia on I_{Ca} depended critically on the cell type expressing slowly or rapidly inactivating Ca^{2+} channels, acidosis effects were independent of cell types. The stronger suppressive effects of hypoxia on slowly inactivating I_{Ca} cells was consistent with the idea that Ca^{2+} dependent inactivation protects the channel against hypoxic suppression (scheme 1), somewhat similar to that found in adult and neonatal rat cardiomyocytes where suppression of CDI by Ba^{2+} [17–19], or Ca^{2+} over-buffering [19] enhanced the hypoxia's suppressive effects. Unexpectedly, hypoxia was more effective in suppressing Ca^{2+} signaling measured at the RyR2 micro-domains rather than in global cytosolic space, suggesting variable effects of hypoxia on calcium signaling pathway.

Development of rapidly and slowly inactivating I_{Ca} in hiPSC-CMs cultures.

In early 4 day cultures of hiPSC-CMs, I_{Ca} magnitude was small and cultures contained similar percentages of rapidly and slowly inactivating L-type I_{Ca} cells (Fig. 1A, C, and D). In older 7–8 day cultures, as the magnitude of I_{Ca} and cell size increased, the cultures appeared to express mostly the slowly inactivating I_{Ca} cell types (Fig. 1B, C and D). This finding is somewhat similar to those of neonatal rat cardiomyocytes where the first 5 days cultures express predominately the rapidly inactivating L-type I_{Ca} cells, while older cultures have predominantly the slowly inactivating I_{Ca} cell types [19, 39]. This is in sharp contrast to I_{Ca} measured in one week old cultures of adult rat cardiomyocytes, where only rapidly inactivating L-type I_{Ca} was measured [17, 18].

Three possible mechanisms were considered to be responsible for the expression of the two kinetically different I_{Ca} cell types: 1) a larger surface to volume ratio in smaller cells of early cultures, where Ca^{2+} influx and release could be more effective in activating CDI than in the older cells with larger volumes (scheme 1); 2) variable expression of molecular determinants of CDI (for instance, CaM, CaM-binding sites and the IQ-like domain) in developing hiPSC-CMs; and 3) culture-age dependent expression of $Ca_V1.2$ and $Ca_V1.3$. Since the inactivation kinetics of I_{Ca} were similarly affected, in hiPSC-CMs with rapidly or slowly inactivating I_{Ca}, when Ba^{2+} was the charge carrier through the Ca^{2+} channels (Fig. 5C) and the tail-current deactivation kinetics of the two cell types were not significantly different (Fig. S1),

variable expression of molecular determinants of CDI was considered unlikely. On the other hand, the linear correlation of cell size and the rate of I_{Ca} inactivation, in more than 150 cells (Fig. 1H), supports the cell size and the ultrastructural proximity of Ca^{2+} stores to plasma membrane as the more likely possibility, see also rN-CMs data [19].

The possibility that the two cardiomyocytes types resulted from differential expression of two calcium channel types, ($Ca_V1.2$ & $Ca_V1.3$), was also not supported by the finding that the level expression of $Ca_V1.2$ mRNA was markedly greater than $Ca_V1.3$ both in the early (day4) or late (day7) cells (Fig. S2). Additionally, the failure of the selective $Ca_V1.3$ antagonist (1-(3-chlorophenethyl)-3-cyclopentylpyrimidine-2,4,6-(1*H*,3*H*,5*H*)-trione) [30] to block I_{Ca} in hiPSC-CMs, where 2 or 10 μM nifedipine produced ~90–95% block of I_{Ca} (panel D of Fig. 2), plus the effectiveness of low concentrations of nifedipine in equally suppressing the current in the two cell types, strongly supports the single rather than two channel types possibility (Fig. 2). Our findings suggest that only $Ca_V1.2$ subtype of L-type calcium channel is expressed in hiPSC-CMs producing 2-different kinetics of inactivation.

Regulation of calcium channels by hypoxia or acidosis in hiPSC-CMs.

Although the consequences of hypoxia and acidosis on I_{Ca} have been studied by a large number of labs in adult rat or guinea-pig ventricular myocytes [17, 18, 36, 40–43] or in rN-CMs [19, 44, 45] very little information has been published about the combined effects of these interventions in modulating I_{Ca} and calcium signaling, especially in hiPSC-CMs [46]. Fig. 4C, D show that the suppressive effect of hypoxia on I_{Ca} varied quantitatively in cells with rapidly or slowly inactivating I_{Ca} (~15% vs. ~45%, respectively). Since the slowly inactivating I_{Ca} hiPSC-CMs are more abundant at the end of first week in culture (~75% vs ~25%), hiPSC-CMs appear to be more vulnerable to acute hypoxia as compared to rA-CMs that express mostly the rapidly inactivating I_{Ca} in the first week of development in culture, showing only ~10–20% hypoxic suppressive effect on I_{Ca} [17, 18]. This disparity in effects of hypoxia on hiPSC-CMs did not occur when Ba^{2+} was the charge carrier through the Ca^{2+} channel (Fig. 5), implying that CDI was critical in protecting against the hypoxic suppression of I_{Ca}. On the other hand, the suppressive effect of acidosis was significantly larger in rapidly inactivating I_{Ca} hiPSC-CMs (~38% vs. ~26%, Fig. 7), in sharp contrast to that reported for rN-CMs where the acidosis suppressive effects were similar in both cell types. In both cell types, there was an initial fast suppression of I_{Ca} in the first 5 seconds of exposure to acute acidosis, presumable caused by binding of protons to the Ca^{2+} permeation site of the channel pore [47–49], and/or neutralizing the membrane surface charges and thereby altering the gating of the channel [50–52]. Note, that this effect was significantly larger in rapidly inactivating I_{Ca} hiPSC-CMs (~22% vs. ~6%, Fig. 7B and F). The slow phase of acidosis suppression of I_{Ca}, following the initial rapid phase, could be the consequence of a smaller but continued acidification (~0.1 pH units) of intracellular milieu in perforated patch clamped conditions, secondary to extracellular acidification, previously reported [53–57].

Although the suppressive effects of ischemia (hypoxia plus acidosis) on I_{Ca} of hiPSC-CMs were equivalent (~45%) in both cell types (Fig. 7B, C, F, G), there was an additive effect of hypoxia plus acidosis in only rapidly inactivating I_{Ca}, suggesting that in addition to blocking

of the channel and heme-oxygenase activation [18], hypoxia may also suppress I_{Ca} by metabolic inhibition of mitochondrial ATP hydrolysis leading to further intracellular acidosis [57, 58] that additionally and differentially suppresses I_{Ca} in the two cell types (scheme 1). The quick and reversible suppressive effects of hypoxia when Ba^{2+} is the charge carrier through the channel (Fig. 5A, B), seen also in rat cardiomyocytes [18, 19, 59], supports the idea that cardiac L-type Ca^{2+} channel can sense O_2 directly through a mechanism independent of the time-dependent activation of, for instance, ROS, hypoxia-inducible factors (HIF), ADP or ATP. Even though the molecular nature of this rapid O_2 sensing mechanism remains not fully understood, the finding that heme-oxygenase 2 (HO-2) inhibitors block the suppressive effects of hypoxia on I_{Ca} is consistent with the possibility that heme-oxgenase bound to CaM/CaMKII binding motif of C-carboxyl terminal of L-type Ca^{2+} channel may render the channel O_2 sensitive [18]. The finding that specific inhibitors of HO-2 and CaMKII, similarly and reversibly suppressed I_{Ca} in hiPSC-CMs as hypoxia, i.e. producing similar I_{Ca} blocking pattern without additive effects (Fig. S6), suggests the same pathway might be involved in the I_{Ca} suppression.

Acidosis and hypoxia modulation of calcium signaling.

In hiPSC-CMs incubated with the Fluo-4 AM, to measure global cytosolic Ca^{2+}, acidosis or hypoxia had a proportional effect on I_{Ca}-triggered Ca^{2+} release as expected from its direct suppressive effect on I_{Ca} and CICR (Fig. S3,F, L), consistent with rN-CMs, where acidosis or hypoxia had a small effect on I_{Ca}-triggered Ca^{2+} release [19]. On the other hand, in hiPSC-CMs infected with genetically engineered probes (GCaMP6-FKBP), to measure RyR2 Ca^{2+} microdomains, acidosis (Fig. S4 I) or hypoxia (Fig. S5 I) alone suppressed the focal Ca^{2+}-transients to a greater extent than that expected from suppression of I_{Ca}. The average reduction in the SR Ca^{2+} content, calculated from the integral of the caffeine-activated I_{NCX}, during acidosis or hypoxia (Figs. S4 L and S5 L) was proportional to the suppression of I_{Ca} (Figs. S4 I and S5 I, lower dot plots) and its accompanying Ca^{2+}-transients (Figs. S4 I and S5 I, upper dot plots) for both cell types. Unexpectedly, only in the slowly inactivating I_{Ca} hiPSC-CMs there was a significant reduction in the SR Ca^{2+} content by acidosis and hypoxia (Figs. S4 L and S5 L). The suppression of focal Ca^{2+}, but not global Ca^{2+}, signals by hypoxia or acidosis appears to be consistent with suppressive effects of these interventions on SR Ca^{2+} content and suggests that focal Ca^{2+}-transients may better represent the pathophysiological regulation of CICR. Extracellular acidosis also modulated I_{Ca} gating and slowed the activation of I_{Ca} in hiPSC-CMs (Fig. S3A, B and S4 A, E) consistent with previous reports in rabbit and guinea pig ventricular myocytes [48, 60, 61] as it delayed the activation of I_{NCX} and their corresponding calcium transients (Fig. S4B, D, F, H).

Beta-adrenergic modulation of hypoxic effects.

In adult guinea pig ventricular cardiomyocytes, hypoxia enhances the affectability of the L-type Ca^{2+} channel to the β-adrenergic agonists [36]. In sharp contrast in rN-CMs [19], or adult rat cardiomyocytes [17, 18], isoproterenol application under hypoxic conditions suppressed rather than desensitized I_{Ca} against hypoxia. In support of these results metabolic inhibition such as ischemia, almost completely suppressed I_{Ca} that was enhanced by β-adrenergic agonist isoproterenol in adult frog cardiomyocytes [57]. In hiPSC-CMs even

though ISO enhanced I_{Ca} significantly (~90%) in both cell types (Fig. 6C, D), β-adrenergic phosphorylation did not protect the channel against hypoxia either in rapidly inactivating I_{Ca} (~ 17% in control vs. ~37% suppression in ISO) or in slowly inactivating cell types (~50% suppression of I_{Ca} in control or phosphorylated channels) Fig. 6. The phosphorylation of L-type Ca^{2+} channel in normoxic conditions reduced significantly the τ_i of the I_{Ca} (~36%) only in the slowly inactivating I_{Ca} hiPSC-CMs, but hypoxia reversed this effect (Fig. 6A, B and F), this may result from β-adrenergic phosphorylation accelerating and synchronizing cardiac RyR2 response per unit of single L-type Ca^{2+} channel [62], making CICR more efficient and enhancing CDI. Since rapidly inactivating I_{Ca} hiPSC-CMs appear to be more resistant to hypoxia, it is likely that the enhancement of CDI may also desensitize the channel to hypoxia. It remains unclear as to why ISO has a significantly different time-dependent effect in culture of hiPSC-CMs (Fig. 1I) when the density of I_{Ca} remains unchanged (Fig. 1E).

Physiological and Biophysical implications.

It is generally assumed that hiPSC-CM cultures have mixed cellular populations, representing atrial, ventricular, and conducting/pacemaker cells. These assumptions are primarily based on measured action potential morphologies: i.e. longer action potentials with prominent plateaus are assumed to be ventricular, while those with shorter plateau phases are identified as atrial, and those showing diastolic depolarization as pacemaker/conducting cells. In fact, this classification is arbitrary and might be misleading, because: 1) Recording of action potential using patch pipette is invasive and may critically alter the native intracellular milieu and create leaks and cellular run down. If the action potential is to be measured reliably, great care must be taken not to introduce holding current from the amplifier, a difficult undertaking unless ultra-tight giga-seal is achieved in current-clamp recording mode [63–67]; 2) there is likely to be more than one cell population based on expression of rapidly and slowly inactivating I_{Ca} (Fig 1 and 3, scheme 1); 3) variability in cell size, and juxtaposition of SR Ca^{2+} store element *vis-a-vis* sarcolemmal I_{Ca} will also affect the action potential morphology (scheme 1); 4) The robust Ca^{2+} signaling and very low expression of Ik_1 in hiPSC-CMs would trigger spontaneous beating characteristics that are often associated with pacemaking/conducting cells. Thus, the variability in action potential morphology is more likely to arise from variability in cellular morphology and I_{Ca} kinetics regulated, in part, by the intracellular Ca^{2+} stores, than by the developmental origins of the myocytes (scheme 1). In this sense, we present new evidence that heterogeneous hiPSC-CMs populations previously reported to reflect atrial and ventricular cell types based on the differences of their APs morphology are most likely caused by the I_{Ca} decay kinetics in a homogenous, but growing cell population (Fig. 3), rather than cell ancestry.

Although differential expression of $Ca_V1.2$ and $Ca_V1.3$ could in part be responsible for the two cell-type populations described above, our pharmacological intervention as well as mRNA expression levels measurements do not support this possibility. The more likely possibility is the changes in cellular morphology and the expression levels of SR Ca^{2+} stores with cell growth in culture vis-a-vis the surface membrane expression of I_{Ca} that produces the two cell populations [19, 68–71]. This and previously published works suggest that Ca^{2+} dependent inactivation protects the channel against hypoxic suppression. This mechanism is

not only regulated by the proximity of SR Ca^{2+} pools to the sarcolemmal L-type Ca^{2+} channels, but also by the mitochondria contribution to the intracellular calcium homeostasis that critically determines the variability of inactivation kinetics and thereby the degree to which the myocyte is affected by hypoxia.

Supplementary Material

Refer to Web version on PubMed Central for supplementary material.

Acknowledgments:

We thank Brittany Henry for general technical help. This work was supported by the National Institute of Health grants to M.M.: (1) NIHR01 HL15162, (2) NIHR01 HL107600.

LIST OF ABBREVIATIONS

APs	action potentials
$[Ca^{2+}]_i$	intracellular calcium-concentration
CDI	calcium-dependent inactivation
CICR	calcium-induced calcium release
FKBP-GCaMP6	RyR2-targeted Ca^{2+} biosensor
hiPSC-CMs	human induced pluripotent stem cell-derived cardiomyocytes
I_{Ca}	calcium current
ISO	Isoproterenol
ROS	reactive oxygen species
Rn-CMs	rat neonatal ventricular cardiomyocytes
RYR	ryanodine receptor
SR	sarcoplasmic reticulum

REFERENCES

[1]. Roth GA, Johnson C, Abajobir A, Abd-Allah F, Abera SF, Abyu G, Ahmed M, Aksut B, Alam T, Alam K, Alla F, Alvis-Guzman N, Amrock S, Ansari H, Arnlov J, Asayesh H, Atey TM, Avila-Burgos L, Awasthi A, Banerjee A, Barac A, Barnighausen T, Barregard L, Bedi N, Belay Ketema E, Bennett D, Berhe G, Bhutta Z, Bitew S, Carapetis J, Carrero JJ, Malta DC, Castaneda-Orjuela CA, Castillo-Rivas J, Catala-Lopez F, Choi JY, Christensen H, Cirillo M, Cooper L, Jr., Criqui M, Cundiff D, Damasceno A, Dandona L, Dandona R, Davletov K, Dharmaratne S, Dorairaj P, Dubey M, Ehrenkranz R, El Sayed Zaki M, Faraon EJA, Esteghamati A, Farid T, Farvid M, Feigin V, Ding EL, Fowkes G, Gebrehiwot T, Gillum R, Gold A, Gona P, Gupta R, Habtewold TD, Hafezi-Nejad N, Hailu T, Hailu GB, Hankey G, Hassen HY, Abate KH, Havmoeller R, Hay SI, Horino M, Hotez PJ, Jacobsen K, James S, Javanbakht M, Jeemon P, John D, Jonas J, Kalkonde Y, Karimkhani C, Kasaeian A, Khader Y, Khan A, Khang YH, Khera S, Khoja AT,

Khubchandani J, Kim D, Kolte D, Kosen S, Krohn KJ, Kumar GA, Kwan GF, Lal DK, Larsson A, Linn S, Lopez A, Lotufo PA, El Razek HMA, Malekzadeh R, Mazidi M, Meier T, Meles KG, Mensah G, Meretoja A, Mezgebe H, Miller T, Mirrakhimov E, Mohammed S, Moran AE, Musa KI, Narula J, Neal B, Ngalesoni F, Nguyen G, Obermeyer CM, Owolabi M, Patton G, Pedro J, Qato D, Qorbani M, Rahimi K, Rai RK, Rawaf S, Ribeiro A, Safiri S, Salomon JA, Santos I, Santric Milicevic M, Sartorius B, Schutte A, Sepanlou S, Shaikh MA, Shin MJ, Shishehbor M, Shore H, Silva DAS, Sobngwi E, Stranges S, Swaminathan S, Tabares-Seisdedos R, Tadele Atnafu N, Tesfay F, Thakur JS, Thrift A, Topor-Madry R, Truelsen T, Tyrovolas S, Ukwaja KN, Uthman O, Vasankari T, Vlassov V, Vollset SE, Wakayo T, Watkins D, Weintraub R, Werdecker A, Westerman R, Wiysonge CS, Wolfe C, Workicho A, Xu G, Yano Y, Yip P, Yonemoto N, Younis M, Yu C, Vos T, Naghavi M, Murray C, Global, Regional, and National Burden of Cardiovascular Diseases for 10 Causes, 1990 to 2015, J Am Coll Cardiol, 70 (2017) 1–25. [PubMed: 28527533]

[2]. Kawaguchi N, Nakanishi T, Cardiomyocyte regeneration, Cells, 2 (2013) 67–82. [PubMed: 24709645]

[3]. Braam SR, Passier R, Mummery CL, Cardiomyocytes from human pluripotent stem cells in regenerative medicine and drug discovery, Trends Pharmacol Sci, 30 (2009) 536–545. [PubMed: 19762090]

[4]. Rajala K, Pekkanen-Mattila M, Aalto-Setala K, Cardiac differentiation of pluripotent stem cells, Stem Cells Int, 2011 (2011) 383709. [PubMed: 21603143]

[5]. Don CW, Murry CE, Improving survival and efficacy of pluripotent stem cell-derived cardiac grafts, J Cell Mol Med, 17 (2013) 1355–1362. [PubMed: 24118766]

[6]. Bers DM, Cardiac excitation-contraction coupling, Nature, 415 (2002) 198–205. [PubMed: 11805843]

[7]. Zhang XH, Haviland S, Wei H, Saric T, Fatima A, Hescheler J, Cleemann L, Morad M, Ca2+ signaling in human induced pluripotent stem cell-derived cardiomyocytes (iPS-CM) from normal and catecholaminergic polymorphic ventricular tachycardia (CPVT)-afflicted subjects, Cell Calcium, 54 (2013) 57–70. [PubMed: 23684427]

[8]. Li S, Cheng H, Tomaselli GF, Li RA, Mechanistic basis of excitation-contraction coupling in human pluripotent stem cell-derived ventricular cardiomyocytes revealed by Ca^{2+} spark characteristics: direct evidence of functional Ca^{2+}-induced Ca^{2+} release, Heart Rhythm, 11 (2014) 133–140. [PubMed: 24096168]

[9]. Zhang XH, Wei H, Saric T, Hescheler J, Cleemann L, Morad M, Regionally diverse mitochondrial calcium signaling regulates spontaneous pacing in developing cardiomyocytes, Cell Calcium, 57 (2015) 321–336. [PubMed: 25746147]

[10]. Hadley RW, Lederer WJ, Ca^{2+} and voltage inactivate Ca^{2+} channels in guinea-pig ventricular myocytes through independent mechanisms, J Physiol, 444 (1991) 257–268. [PubMed: 1668348]

[11]. van der Heyden MA, Wijnhoven TJ, Opthof T, Molecular aspects of adrenergic modulation of cardiac L-type Ca^{2+} channels, Cardiovasc Res, 65 (2005) 28–39. [PubMed: 15621031]

[12]. Striessnig J, Ortner NJ, Pinggera A, Pharmacology of L-type Calcium Channels: Novel Drugs for Old Targets?, Curr Mol Pharmacol, 8 (2015) 110–122. [PubMed: 25966690]

[13]. Bauwens C, Yin T, Dang S, Peerani R, Zandstra PW, Development of a perfusion fed bioreactor for embryonic stem cell-derived cardiomyocyte generation: oxygen-mediated enhancement of cardiomyocyte output, Biotechnol Bioeng, 90 (2005) 452–461. [PubMed: 15778986]

[14]. Niebruegge S, Bauwens CL, Peerani R, Thavandiran N, Masse S, Sevaptisidis E, Nanthakumar K, Woodhouse K, Husain M, Kumacheva E, Zandstra PW, Generation of human embryonic stem cell-derived mesoderm and cardiac cells using size-specified aggregates in an oxygen-controlled bioreactor, Biotechnol Bioeng, 102 (2009) 493–507. [PubMed: 18767184]

[15]. Horton RE, Auguste DT, Synergistic effects of hypoxia and extracellular matrix cues in cardiomyogenesis, Biomaterials, 33 (2012) 6313–6319. [PubMed: 22717366]

[16]. Correia C, Serra M, Espinha N, Sousa M, Brito C, Burkert K, Zheng Y, Hescheler J, Carrondo MJ, Saric T, Alves PM, Combining hypoxia and bioreactor hydrodynamics boosts induced pluripotent stem cell differentiation towards cardiomyocytes, Stem Cell Rev, 10 (2014) 786–801. [PubMed: 25022569]

[17]. Movafagh S, Morad M, L-type calcium channel as a cardiac oxygen sensor, Ann N Y Acad Sci, 1188 (2010) 153–158. [PubMed: 20201898]

[18]. Rosa AO, Movafagh S, Cleemann L, Morad M, Hypoxic regulation of cardiac Ca^{2+} channel: possible role of haem oxygenase, J Physiol, 590 (2012) 4223–4237. [PubMed: 22753548]

[19]. Fernandez-Morales JC, Morad M, Regulation of Ca(2+) signaling by acute hypoxia and acidosis in rat neonatal cardiomyocytes, J Mol Cell Cardiol, 114 (2018) 58–71. [PubMed: 29032102]

[20]. Si-Tayeb K, Noto FK, Sepac A, Sedlic F, Bosnjak ZJ, Lough JW, Duncan SA, Generation of human induced pluripotent stem cells by simple transient transfection of plasmid DNA encoding reprogramming factors, BMC Dev Biol, 10 (2010) 81. [PubMed: 20682060]

[21]. Lian X, Zhang J, Azarin SM, Zhu K, Hazeltine LB, Bao X, Hsiao C, Kamp TJ, Palecek SP, Directed cardiomyocyte differentiation from human pluripotent stem cells by modulating Wnt/beta-catenin signaling under fully defined conditions, Nat Protoc, 8 (2013) 162–175. [PubMed: 23257984]

[22]. Lindau M, Fernandez JM, A patch-clamp study of histamine-secreting cells, J Gen Physiol, 88 (1986) 349–368. [PubMed: 2428921]

[23]. Horn R, Marty A, Muscarinic activation of ionic currents measured by a new whole-cell recording method, J Gen Physiol, 92 (1988) 145–159. [PubMed: 2459299]

[24]. Aggett PJ, Fenwick PK, Kirk H, The effect of amphotericin B on the permeability of lipid bilayers to divalent trace metals, Biochim Biophys Acta, 684 (1982) 291–294. [PubMed: 7055571]

[25]. Rae J, Cooper K, Gates P, Watsky M, Low access resistance perforated patch recordings using amphotericin B, J Neurosci Methods, 37 (1991) 15–26. [PubMed: 2072734]

[26]. Lieu DK, Liu J, Siu CW, McNerney GP, Tse HF, Abu-Khalil A, Huser T, Li RA, Absence of transverse tubules contributes to non-uniform Ca(2+) wavefronts in mouse and human embryonic stem cell-derived cardiomyocytes, Stem Cells Dev, 18 (2009) 1493–1500. [PubMed: 19290776]

[27]. Satin J, Itzhaki I, Rapoport S, Schroder EA, Izu L, Arbel G, Beyar R, Balke CW, Schiller J, Gepstein L, Calcium handling in human embryonic stem cell-derived cardiomyocytes, Stem Cells, 26 (2008) 1961–1972. [PubMed: 18483424]

[28]. Satoh H, Delbridge LM, Blatter LA, Bers DM, Surface:volume relationship in cardiac myocytes studied with confocal microscopy and membrane capacitance measurements: species-dependence and developmental effects, Biophys J, 70 (1996) 1494–1504. [PubMed: 8785306]

[29]. Cleemann L, Morad M, Role of Ca^{2+} channel in cardiac excitation-contraction coupling in the rat: evidence from Ca^{2+} transients and contraction, J Physiol, 432 (1991) 283–312. [PubMed: 1653321]

[30]. Kang S, Cooper G, Dunne SF, Dusel B, Luan CH, Surmeier DJ, Silverman RB, CaV1.3-selective L-type calcium channel antagonists as potential new therapeutics for Parkinson's disease, Nat Commun, 3 (2012) 1146. [PubMed: 23093183]

[31]. Koschak A, Reimer D, Huber I, Grabner M, Glossmann H, Engel J, Striessnig J, alpha 1D (Cav1.3) subunits can form l-type Ca2+ channels activating at negative voltages, J Biol Chem, 276 (2001) 22100–22106. [PubMed: 11285265]

[32]. Carbone E, Lux HD, Kinetics and selectivity of a low-voltage-activated calcium current in chick and rat sensory neurones, J Physiol, 386 (1987) 547–570. [PubMed: 2445968]

[33]. Nilius B, Hess P, Lansman JB, Tsien RW, A novel type of cardiac calcium channel in ventricular cells, Nature, 316 (1985) 443–446. [PubMed: 2410797]

[34]. Hulme JT, Westenbroek RE, Scheuer T, Catterall WA, Phosphorylation of serine 1928 in the distal C-terminal domain of cardiac CaV1.2 channels during beta1-adrenergic regulation, Proc Natl Acad Sci U S A, 103 (2006) 16574–16579. [PubMed: 17053072]

[35]. Haase H, Bartel S, Karczewski P, Morano I, Krause EG, In-vivo phosphorylation of the cardiac L-type calcium channel beta-subunit in response to catecholamines, Mol Cell Biochem, 163–164 (1996) 99–106.

[36]. Hool LC, Hypoxia alters the sensitivity of the L-type Ca(2+) channel to alpha-adrenergic receptor stimulation in the presence of beta-adrenergic receptor stimulation, Circ Res, 88 (2001) 1036–1043. [PubMed: 11375273]

[37]. Williamson JR, Schaffer SW, Ford C, Safer B, Contribution of tissue acidosis to ischemic injury in the perfused rat heart, Circulation, 53 (1976) I3–14. [PubMed: 3293]

[38]. Varro A, Hester S, Papp JG, Caffeine-induced decreases in the inward rectifier potassium and the inward calcium currents in rat ventricular myocytes, Br J Pharmacol, 109 (1993) 895–897. [PubMed: 8401940]

[39]. Gomez JP, Potreau D, Branka JE, Raymond G, Developmental changes in Ca2+ currents from newborn rat cardiomyocytes in primary culture, Pflugers Arch, 428 (1994) 241–249. [PubMed: 7816546]

[40]. Poole-Wilson PA, Acidosis and contractility of heart muscle, Ciba Found Symp, 87 (1982) 58–76. [PubMed: 6804193]

[41]. Orchard CH, Cingolani HE, Acidosis and arrhythmias in cardiac muscle, Cardiovasc Res, 28 (1994) 1312–1319. [PubMed: 7954638]

[42]. Komukai K, Brette F, Pascarel C, Orchard CH, Electrophysiological response of rat ventricular myocytes to acidosis, Am J Physiol Heart Circ Physiol, 283 (2002) H412–422. [PubMed: 12063316]

[43]. Wolkart G, Schrammel A, Koyani CN, Scherubel S, Zorn-Pauly K, Malle E, Pelzmann B, Andra M, Ortner A, Mayer B, Cardioprotective effects of 5-hydroxymethylfurfural mediated by inhibition of L-type Ca(2+) currents, Br J Pharmacol, 174 (2017) 3640–3653. [PubMed: 28768052]

[44]. Gonzalez-Rodriguez P, Falcon D, Castro MJ, Urena J, Lopez-Barneo J, Castellano A, Hypoxic induction of T-type Ca(2+) channels in rat cardiac myocytes: role of HIF-1alpha and RhoA/ROCK signalling, J Physiol, 593 (2015) 4729–4745. [PubMed: 26331302]

[45]. Martewicz S, Michielin F, Serena E, Zambon A, Mongillo M, Elvassore N, Reversible alteration of calcium dynamics in cardiomyocytes during acute hypoxia transient in a microfluidic platform, Integr Biol (Camb), 4 (2012) 153–164. [PubMed: 22158991]

[46]. Wei W, Liu Y, Zhang Q, Wang Y, Zhang X, Zhang H, Danshen-Enhanced Cardioprotective Effect of Cardioplegia on Ischemia Reperfusion Injury in a Human-Induced Pluripotent Stem Cell-Derived Cardiomyocytes Model, Artif Organs, 41 (2017) 452–460. [PubMed: 27925238]

[47]. Prod'hom B, Pietrobon D, Hess P, Interactions of protons with single open L-type calcium channels. Location of protonation site and dependence of proton-induced current fluctuations on concentration and species of permeant ion, J Gen Physiol, 94 (1989) 23–42. [PubMed: 2553858]

[48]. Krafte DS, Kass RS, Hydrogen ion modulation of Ca channel current in cardiac ventricular cells. Evidence for multiple mechanisms, J Gen Physiol, 91 (1988) 641–657. [PubMed: 2458428]

[49]. Klockner U, Isenberg G, Calcium channel current of vascular smooth muscle cells: extracellular protons modulate gating and single channel conductance, J Gen Physiol, 103 (1994) 665–678. [PubMed: 8057083]

[50]. Katzka DA, Morad M, Properties of calcium channels in guinea-pig gastric myocytes, J Physiol, 413 (1989) 175–197. [PubMed: 2557436]

[51]. Ohmori H, Yoshii M, Surface potential reflected in both gating and permeation mechanisms of sodium and calcium channels of the tunicate egg cell membrane, J Physiol, 267 (1977) 429–463. [PubMed: 17734]

[52]. Iijima T, Ciani S, Hagiwara S, Effects of the external pH on Ca channels: experimental studies and theoretical considerations using a two-site, two-ion model, Proc Natl Acad Sci U S A, 83 (1986) 654–658. [PubMed: 2418439]

[53]. Matsuda N, Mori T, Nakamura H, Shigekawa M, Mechanisms of reoxygenation-induced calcium overload in cardiac myocytes: dependence on pHi, J Surg Res, 59 (1995) 712–718. [PubMed: 8538170]

[54]. Kaibara M, Kameyama M, Inhibition of the calcium channel by intracellular protons in single ventricular myocytes of the guinea-pig, J Physiol, 403 (1988) 621–640. [PubMed: 2855346]

[55]. Irisawa H, Sato R, Intra- and extracellular actions of proton on the calcium current of isolated guinea pig ventricular cells, Circ Res, 59 (1986) 348–355. [PubMed: 2429781]

[56]. Klockner U, Isenberg G, Intracellular pH modulates the availability of vascular L-type Ca^{2+} channels, J Gen Physiol, 103 (1994) 647–663. [PubMed: 8057082]

[57]. Kanaporis G, Treinys R, Fischmeister R, Jurevicius J, Metabolic inhibition reduces cardiac L-type Ca2+ channel current due to acidification caused by ATP hydrolysis, PLoS One, 12 (2017) e0184246. [PubMed: 28859158]

[58]. Di Lisa F, Blank PS, Colonna R, Gambassi G, Silverman HS, Stern MD, Hansford RG, Mitochondrial membrane potential in single living adult rat cardiac myocytes exposed to anoxia or metabolic inhibition, J Physiol, 486 (Pt 1) (1995) 1–13. [PubMed: 7562625]

[59]. Scaringi JA, Rosa AO, Morad M, Cleemann L, A new method to detect rapid oxygen changes around cells: how quickly do calcium channels sense oxygen in cardiomyocytes?, J Appl Physiol (1985), 115 (2013) 1855–1861. [PubMed: 24157525]

[60]. Saegusa N, Moorhouse E, Vaughan-Jones RD, Spitzer KW, Influence of pH on Ca(2)(+) current and its control of electrical and Ca(2)(+) signaling in ventricular myocytes, J Gen Physiol, 138 (2011) 537–559. [PubMed: 22042988]

[61]. Kwan YW, Kass RS, Interactions between H^+ and Ca^{2+} near cardiac L-type calcium channels: evidence for independent channel-associated binding sites, Biophys J, 65 (1993) 1188–1195. [PubMed: 8241399]

[62]. Zhou P, Zhao YT, Guo YB, Xu SM, Bai SH, Lakatta EG, Cheng H, Hao XM, Wang SQ, Beta-adrenergic signaling accelerates and synchronizes cardiac ryanodine receptor response to a single L-type Ca^{2+} channel, Proc Natl Acad Sci U S A, 106 (2009) 18028–18033. [PubMed: 19815510]

[63]. Zhu R, Millrod MA, Zambidis ET, Tung L, Variability of Action Potentials Within and Among Cardiac Cell Clusters Derived from Human Embryonic Stem Cells, Sci Rep, 6 (2016) 18544. [PubMed: 26729331]

[64]. Warren M, Spitzer KW, Steadman BW, Rees TD, Venable P, Taylor T, Shibayama J, Yan P, Wuskell JP, Loew LM, Zaitsev AV, High-precision recording of the action potential in isolated cardiomyocytes using the near-infrared fluorescent dye di-4-ANBDQBS, Am J Physiol Heart Circ Physiol, 299 (2010) H1271–1281. [PubMed: 20601458]

[65]. Perkins KL, Cell-attached voltage-clamp and current-clamp recording and stimulation techniques in brain slices, J Neurosci Methods, 154 (2006) 1–18. [PubMed: 16554092]

[66]. Sakmann B, Neher E, Patch clamp techniques for studying ionic channels in excitable membranes, Annu Rev Physiol, 46 (1984) 455–472. [PubMed: 6143532]

[67]. Neher E, Sakmann B, The patch clamp technique, Sci Am, 266 (1992) 44–51. [PubMed: 1374932]

[68]. Vornanen M, Excitation-contraction coupling of the developing rat heart, Mol Cell Biochem, 163–164 (1996) 5–11.

[69]. Vornanen M, Contribution of sarcolemmal calcium current to total cellular calcium in postnatally developing rat heart, Cardiovasc Res, 32 (1996) 400–410. [PubMed: 8796128]

[70]. Snopko RM, Aromolaran AS, Karko KL, Ramos-Franco J, Blatter LA, Mejia-Alvarez R, Cell culture modifies Ca^{2+} signaling during excitation-contraction coupling in neonate cardiac myocytes, Cell Calcium, 41 (2007) 13–25. [PubMed: 16908061]

[71]. Ziman AP, Gomez-Viquez NL, Bloch RJ, Lederer WJ, Excitation-contraction coupling changes during postnatal cardiac development, J Mol Cell Cardiol, 48 (2010) 379–386. [PubMed: 19818794]

Highlights

Key Points Summary

- Cardiomyocytes cultures derived from Human Induced Pluripotent Stem Cells (hiPSCCM) express two cell-type populations based on inactivation kinetics of L-type I_{Ca} (tau 20ms & 50ms).
- This differential expression of slowly and rapidly inactivating I_{Ca}, in hiPSC-CM cultures maybe responsible for variability in action potential morphology previously reported in hiPSC-CM cultures and attributed to atrial or ventricular ancestry origins of the cells.
- The suppressive effects of hypoxia were larger in slowly (predominant cell-type in culture) vs rapidly inactivating calcium channels suggesting that rapid calcium dependent inactivation protected the channel against hypoxia.
- Acute hypoxia suppressed I_{Ca} to varied extent and kinetics in both cell-types, but this effect disappeared when Ba^{2+} was the channel charge carrier suggesting critical role for Ca^{2+}-dependent inactivation in the hypoxic response.
- The suppression of focal Ca^{2+}, but not global Ca^{2+} transients by hypoxia or acidosis appears more consistent with suppressive effects of these interventions on SR Ca^{2+} content and suggests that focal rather than global cytosolic Ca^{2+} may better represent the pathophysiological regulation of CICR.

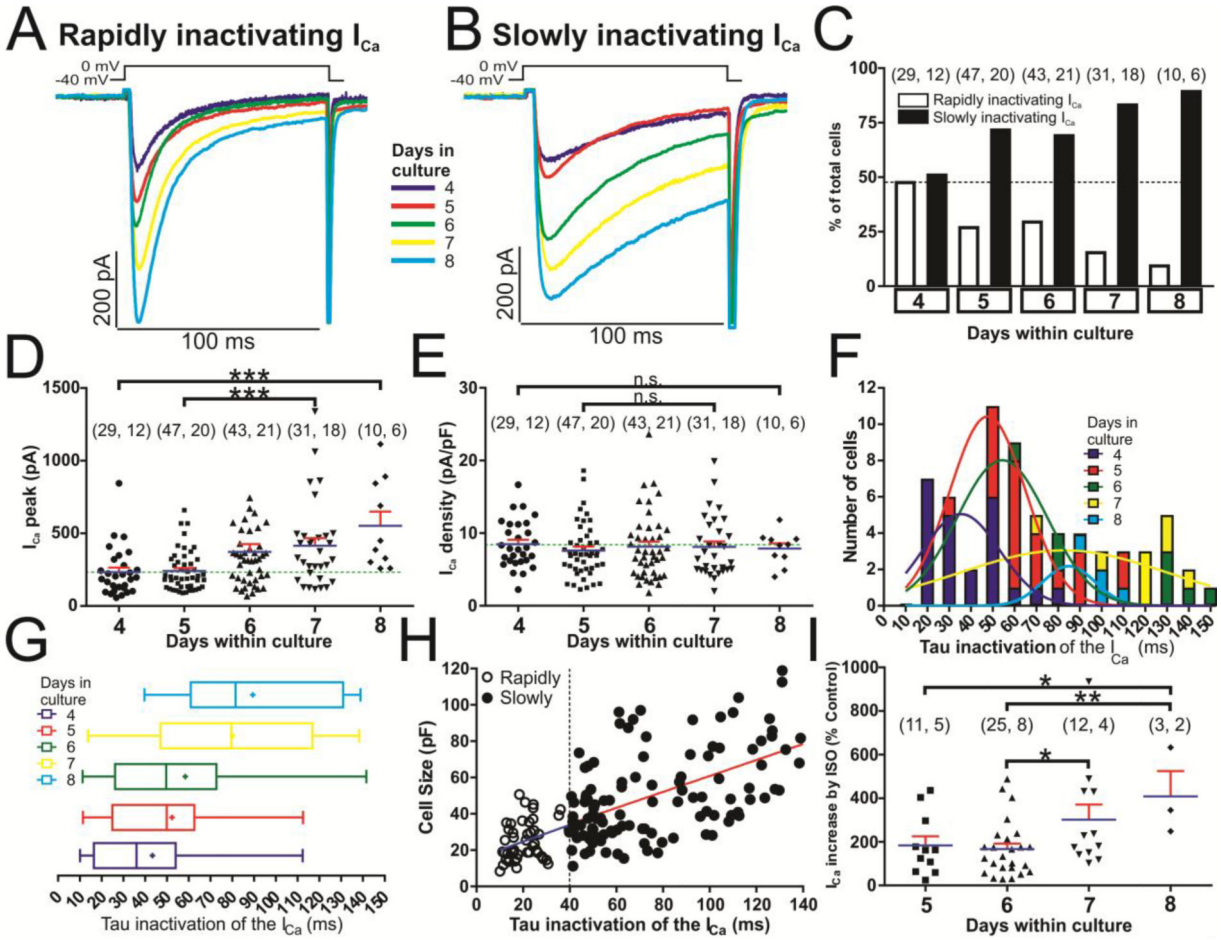

Fig. 1.- Two different time dependent kinetics of L-type calcium channels are expressed in cultured hiPSC-CMs.

Panels A and B show examples of original traces of calcium currents obtained from different hiPSC-CMs with variable ages in culture (4–8 days), activated by depolarization from −40 mV to 0 mV, exhibiting different rates of inactivation: Rapidly inactivating I_{Ca} (Panel A) and slowly inactivating I_{Ca} (Panel B). Panel C shows a plot of the cell percentages that presented rapidly or slowly inactivating I_{Ca} vs. the age of the cells in culture. Panel D and E, presented as dot plots, represent the individual cell values of I_{Ca} and Ca^{2+} current density respectively vs. cell time in culture (4–8 days); the mean is represented by blue bars and the standard error of the mean by the red error bars. Panel F and G provide frequency histograms and box and whiskers plots respectively showing the distribution of the inactivation time constant of the I_{Ca} (τ_i) at the five different time in culture (4, 5, 6, 7 and 8 days). The data were pooled in such a way that the number of observations with 0.00 ms ≤ τ_i < ms were plotted in the column τ_i = 10 ms and in the same way with the rest of observations. The data were fitted to a Normal Distribution with five different colors Gauss curve represented (dark blue, red, green, yellow and light blue for hiPSC-CMs with 4, 5, 6, 7 or 8 days in culture respectively). Data distribution are presented also in box-and-whiskers plots with the same colors/days in culture scheme: the line inside the box depicts median values, the size of the box is given by the distance between the 25th and the 75th percentiles; right “whisker” reach the 90th percentile and left “whisker” the percentile 10th. Means are also represented inside the box

with a cross symbol. Panel H shows a scatter-graph plot of cell size (pF) vs. inactivation time constant (τ_i) from hiPSC-CMs with rapidly (○) and slowly (●) inactivating I_{Ca}, hiPSC-CMs were classified as expressing rapidly- ($\tau_i \leq 40$ ms) or slowly-inactivating ($\tau_i > 40$ ms) L-type Ca^{2+} channels. Panel I is represented as a dot plot, showing the distribution of individual cell values of I_{Ca} increased (in % with respect to the I_{Ca} peak under control conditions without ISO) during the treatment with 100 nM isoproterenol at the time of the cells in culture (5–8 days). In panels C, D, E and I, for each of the different data groups, the number of cells (*n*) and the number of different cultures conducted to obtain these data (N) are indicated in parentheses as (*n*, N). Data were presented as the mean ± SEM in this figure. We used one-way ANOVA with post-hoc multiple comparisons using the Tukey's multiple comparisons test for unpaired parametric comparisons. $*P < 0.05$; $**P < 0.01$; n.s.: not significant.

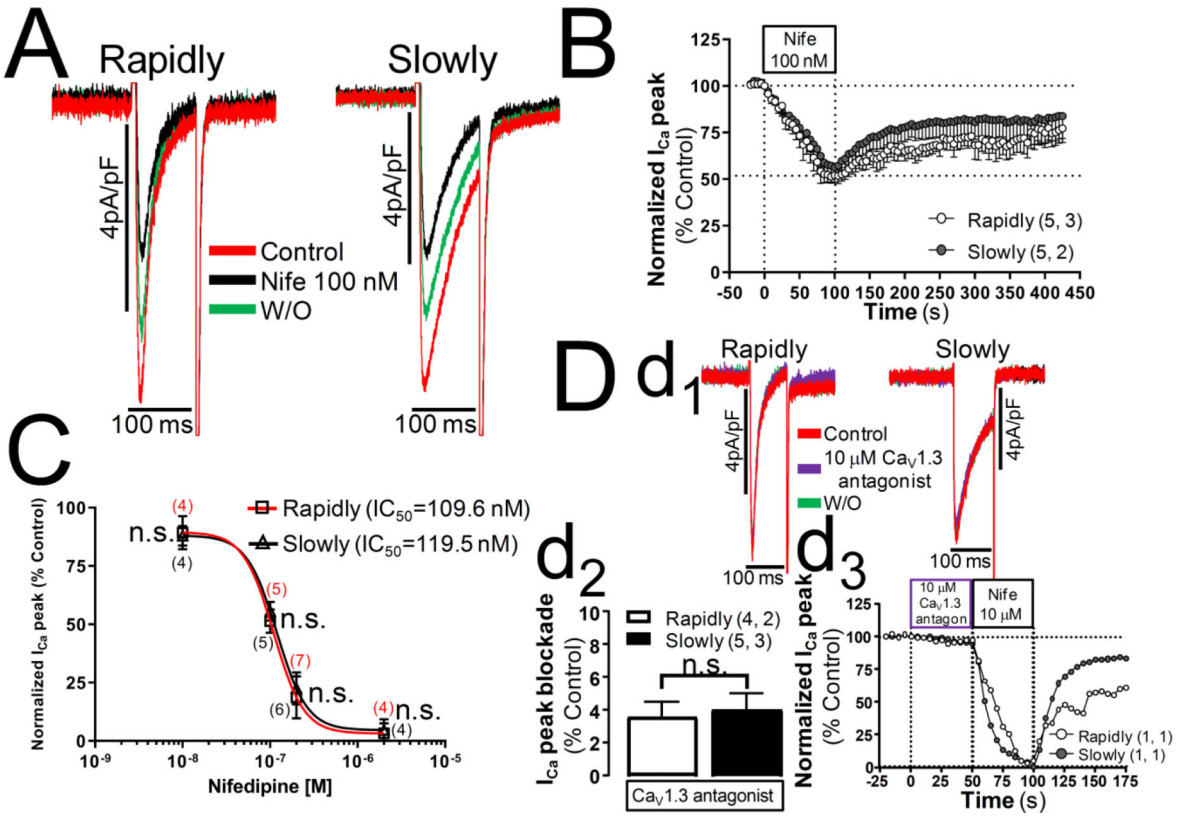

Fig. 2.- Concentration-dependent blockade of the whole-cell Ca^{2+} current elicited by nifedipine and a novel $Ca_V1.3$ antagonist in hiPSC-CMs with different inactivation kinetics.

I_{Ca} was recorded under the perforated-patch mode of the patch-clamp technique using 2 mM Ca^{2+} as charge carrier and calcium currents were elicited by 100 ms depolarization pulses from −40 mV to 0 mV. Panel A show I_{Ca} traces reduced after being perfused during 100 seconds with 100 nM nifedipine from hiPSC-CMs with rapidly and slowly inactivating I_{Ca}. Panel B show the time course of the I_{Ca} blockade elicited by 100 nM nifedipine. In panel C are exposed the concentration-dependent blockade of the whole-cell I_{Ca} peak elicited by nifedipine in hiPSC-CMs with rapidly and slowly inactivating I_{Ca} with its corresponding values of IC_{50}, the sigmoidal concentration-response curves and the number of cells for each of the concentrations of nifedipine (10 nM, 100 nM, 200 nM and 2 μM) are shown in parentheses for rapidly inactivating I_{Ca} cells (red color) and slowly inactivating I_{Ca} cells (black). Panel D show the inapparent effect suppressing I_{Ca} of a novel and selective $Ca_V1.3$ antagonist (1-(3-chlorophenethyl)-3-cyclopentylpyrimidine-2,4,6-(1*H*,3*H*,5*H*)-trione), in the subpanels inserted labeled as d_1 are represented I_{Ca} traces at control level (red traces), 10 μM $Ca_V1.3$ antagonist (purple traces) and normoxia wash out (green traces) belonging to one of the hiPSC-CMs with rapidly inactivating I_{Ca} and another with slowly inactivating I_{Ca}. The subpanel inserted labeled as d_2 plotted the the average blocking effect on I_{Ca} by 10 μM of the $Ca_V1.3$ antagonist in both cell types. Inserted subpanel d_3 show the time course of the blockade effect of I_{Ca} elicited initially by the $Ca_V1.3$ antagonist and then by nifedipine 10 μM from two single cells with rapidly and slowly inactivation kinetics. The number of cells (*n*) and the number of different cultures (N) are indicated as (*n*, N). Data are mean ± SEM. n.s.: not significant; by paired Student's t-test.

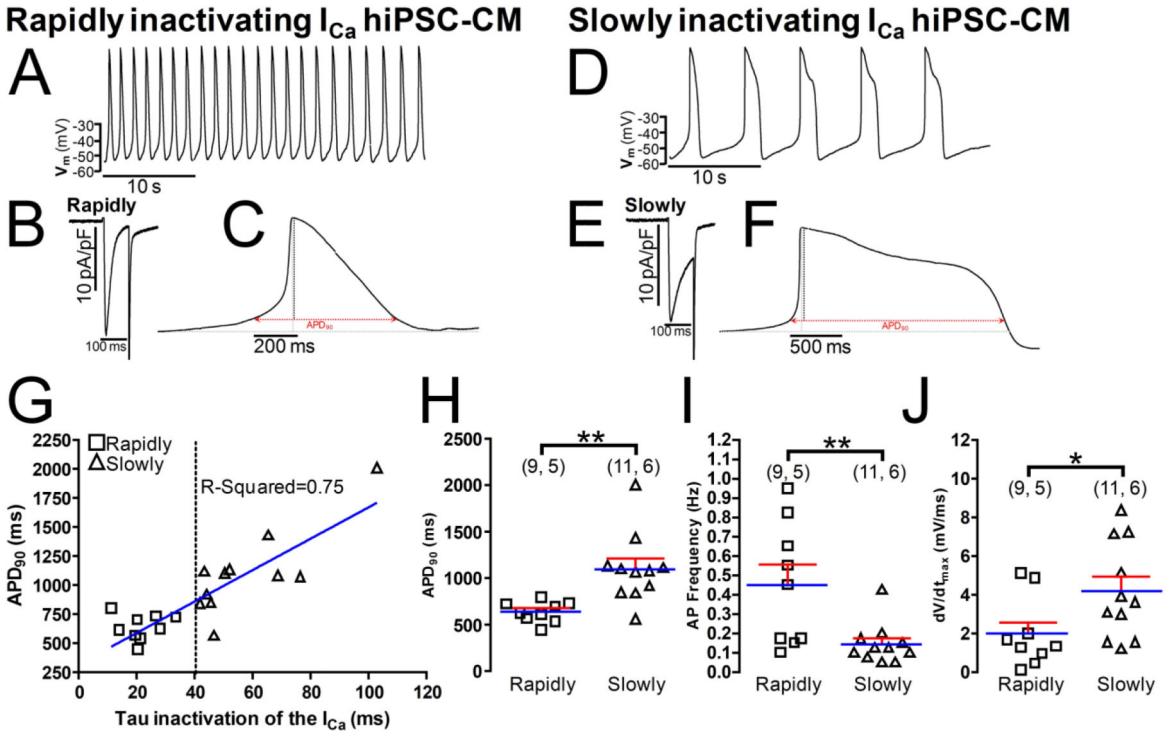

Fig. 3.- Action potentials properties are correlated with the I_{Ca} decay kinetics expressed in heterogeneous hiPSC-CMs populations.

Panels A and D show examples of original traces of the action potentials (APs) spontaneously emitted during 35s by hiPSC-CMs with rapidly or slowly inactivating I_{Ca} respectively. Panels C and F exhibit two samples of singles APs obtained from cells with rapidly and slowly inactivating I_{Ca} and panels B and E display the original I_{Ca} records. Panel G shows a scatter-graph plot of the action potential duration at 90% repolarization (APD_{90}) (ms) vs. inactivation time constant (τ_i) from hiPSC-CMs with rapidly (○) and slowly (●) inactivating I_{Ca}, hiPSC-CMs were classified as expressing rapidly- ($\tau_i \leq 40$ ms) or slowlyinactivating ($\tau_i > 40$ ms) L-type Ca^{2+} channels. Panels H, I and J show the distribution of individual cell values and the average values (blue line) of APD_{90}, AP frequency (Hz) and AP upstroke velocity, dV/dt (mV/ms), respectively from hiPSC-CMs expressing rapidly (squares) or slowly (triangles) inactivating L-type Ca^{2+} channels. In the panels H, I, and J, for each of the different data groups (rapidly or slowly inactivating I_{Ca} cells), the number of cells (*n*) and the number of different cultures conducted to obtain these data (N) are indicated in parentheses as (*n*, N). Data were presented as the mean ± SEM in this figure. $*P < 0.05$; $**P < 0.01$; by unpaired two-tailed Student's t-test in this figure.

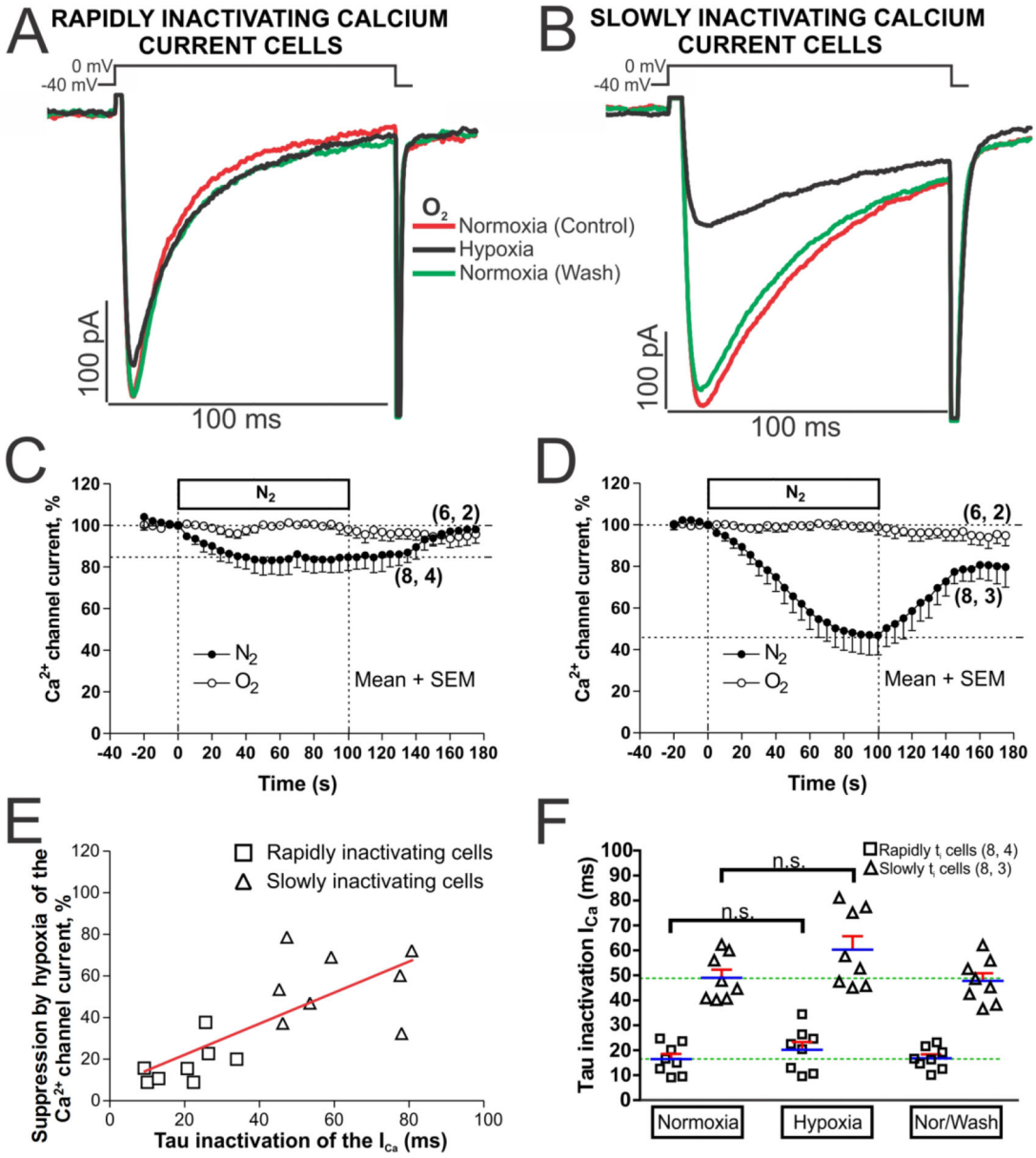

Fig. 4.- Acute hypoxia differentially affects to the hiPSC-CMs with rapidly or slowly inactivating I_{Ca}.

Panels A and B show examples of original traces of calcium currents obtained from two different hiPSC-CMs, activated by depolarization from −40 mV to 0 mV, exhibiting different rates of inactivation as well as differing degrees of suppression during acute hypoxia (black traces). Panels C and D display time courses of suppression of I_{Ca} during 2 minutes of hypoxia stimulus (N_2 top bar, black circles) in hiPSC-CMs with rapidly and slowly inactivating $I_{Ca,}$ respectively. Time courses with white circles represent a set of hiPSC-CMs under normoxic condition during 200 seconds. Panel E shows a scatter-graph of hypoxic suppression of I_{Ca} vs. inactivation time constant (τ_i) from hiPSC-CMs with rapidly (□) and slowly (Δ) inactivating I_{Ca} with the correlation line associate represented in red. Panel F show in a dot plot format the distribution of individual cell values and the average τ_i values

of I_{Ca} (blue line) before, during, and after exposure to hypoxia for each of the two cell types. In the panels C, D, and F, for each one of the different data groups, the number of cells (*n*) and the number of different cultures conducted to obtain these data (N) are indicated in parentheses as (*n*, N). Data were presented as the mean ± SEM in this figure. n.s.: not significant; by paired two-tailed Student's t-test in this figure.

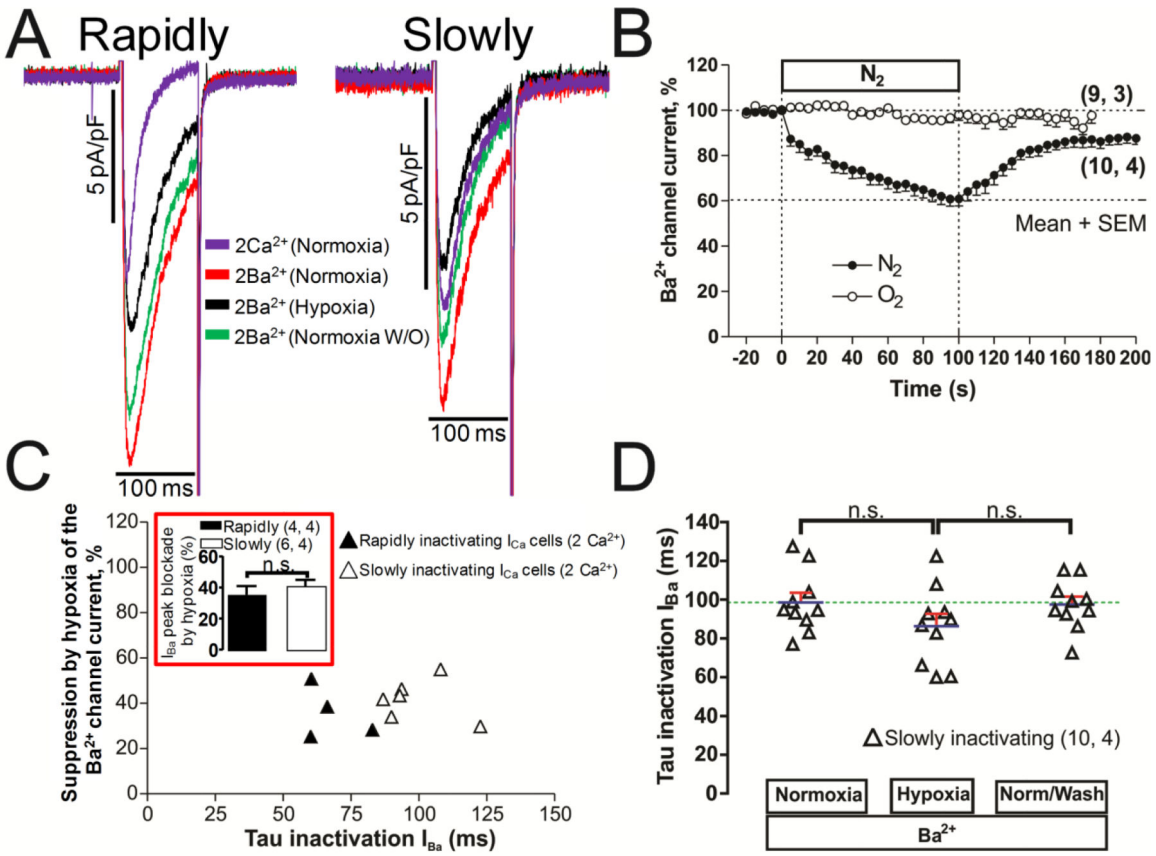

Fig. 5.- Cardiac L-type Ca^{2+} channel suppression by acute hypoxia whit Ba^{2+} as charge carrier. Panels A show examples of original traces of rapidly and slowly inactivating I_{Ca} hiPSC-CMs in the presence of 2 mM Ca^{2+} (purple) that becomes slowly inactivating when we shifted the extracellular charge carrier to 2 mM Ba^{2+} in normoxia condition (red traces). The cells were activated by depolarization from −40 mV to 0 mV and exposed to acute hypoxia (black traces) and normoxia washout (green traces). Panel B displayed the time course of suppression of I_{Ba} during 100 s by hypoxia stimulus (N_2 top bar) in a set of hiPSC-CMs. Panel C shows a scattergraph plot of the hypoxic suppression degree of I_{Ba} vs. inactivation time constant (τ_i) of I_{Ba} traces from hiPSC-CMs just after 100 s of hypoxia, with black or white triangles are distinguished the cells that have rapidly or slowly inactivating I_{Ca} in the presence of 2 mM Ca^{2+}, the red insert box represent the average blockade by hypoxia in the presence of extracellular Ba^{2+} in cells with rapidly or slowly inactivating I_{Ca}. Panel D show, in dot plot format, the distribution of individual cell values and the average τ_i values of I_{Ba} (blue line) before, during, and after exposure to hypoxia. In the panels B, C and D, for each one of the different data groups, the number of cells (*n*) and the number of different cultures conducted to obtain these data (N) are indicated in parentheses as (*n*, N). Data were presented as the mean ± SEM in this figure. n.s.: not significant; by paired two-tailed Student's t-test in this figure.

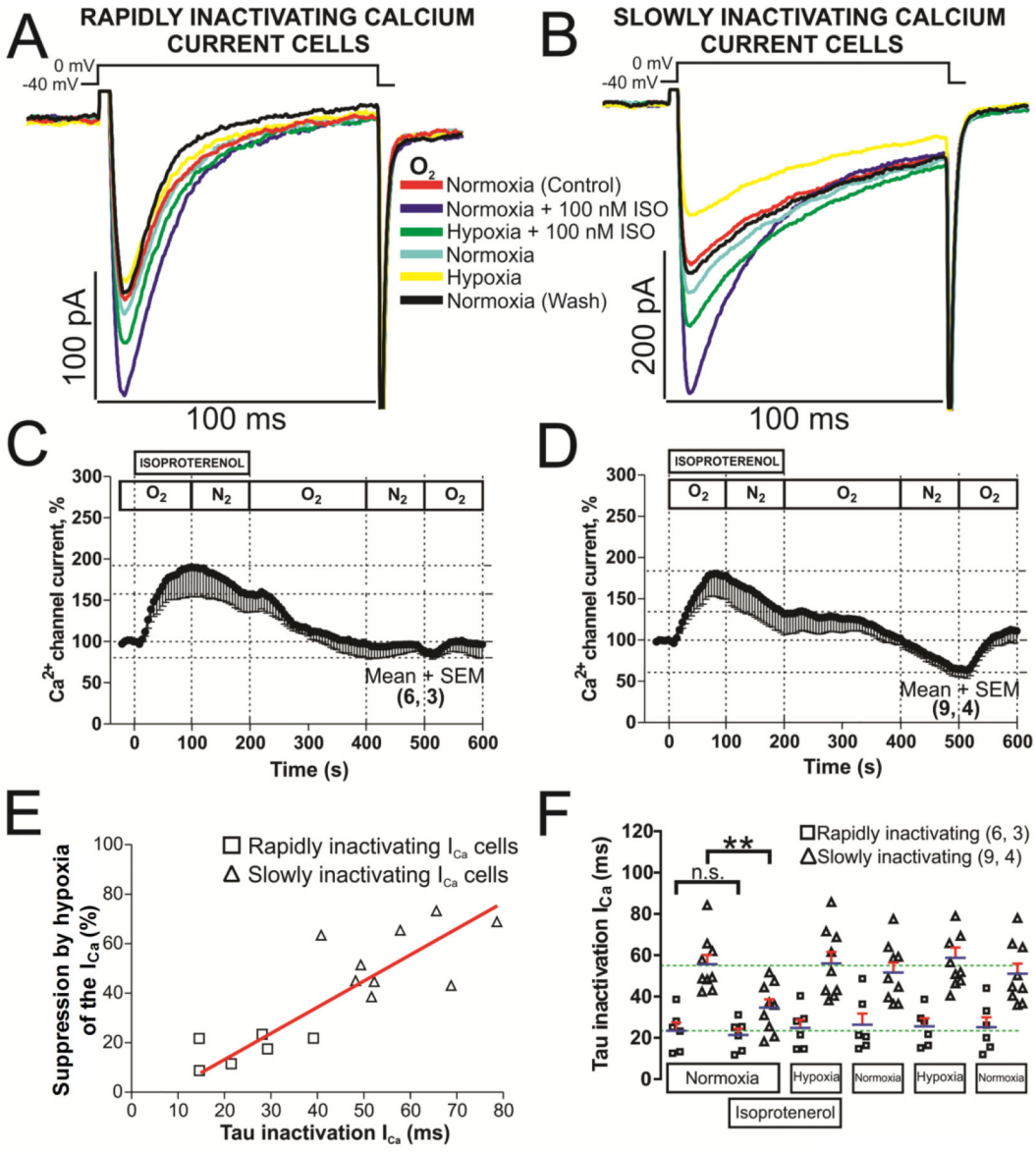

Fig. 6.- Phosphorylation effects of isoproterenol (ISO) on calcium channels of hiPSC-CMs with rapidly or slowly inactivating I_{Ca} in normoxia and hypoxia conditions.

Panels A and B show examples of original traces of rapidly and slowly inactivating I_{Ca} respectively, obtained from two different hiPSC-CMs, activated by depolarization from −40 mV to 0 mV and exposed to the following consecutive treatments: 1) red traces, normoxia control condition; 2) dark blue traces, initial treatment with 100 nM ISO in normoxia; 3) green traces, shift to the hypoxic condition maintaining the ISO treatment; 4) light blue traces, return to the normoxia condition after ISO washout; 5) yellow traces, second subsequent hypoxia stimulation without ISO, 6) black traces, final return to the normoxia condition. Panels C and D displayed time courses (in hiPSC-CMs with rapidly and slowly inactivating $I_{Ca,}$ respectively) of modulation of I_{Ca} by ISO perfused during 200 s (ISO bar) at the consecutives conditions of normoxia and hypoxia, represented by the sequence of O_2 and N_2 top bars, respectively. Panel E shows a scatter-graph plot of hypoxic suppression of

I_{Ca} vs. τ_i from hiPSC-CMs with rapidly (□) and slowly (Δ) inactivating I_{Ca} with the respective correlation line found represented in red. Panel F shows, in a dot plot format, the distribution of individual cell values and the average τ_i values of I_{Ca} (blue lines with SEM represented by red error bars) under normoxic and hypoxic conditions with or without ISO for each of the two cell types. Note here that the plotted data in the temporary course have a consider standard error of the mean (SEM) during the ISO treatment in both cell types due to the large variability that has ISO enhancing I_{Ca} in hiPSC-CMs (different aspect as we found in rN-CMs) and how this error is reduced as the washout of the ISO progresses (final part of the temporary course of the panels C and D). In the panels C, D, and F, for each one of the different data groups, the number of cells (*n*) and the number of different cultures conducted to obtain these data (N) are indicated in parentheses as (*n*, N). Data were presented as the mean ± SEM in this figure. $^{**}P < 0.01$; n.s.: not significant; by paired two-tailed Student's t-test in this figure. Mann-Whitney rank-sum test.

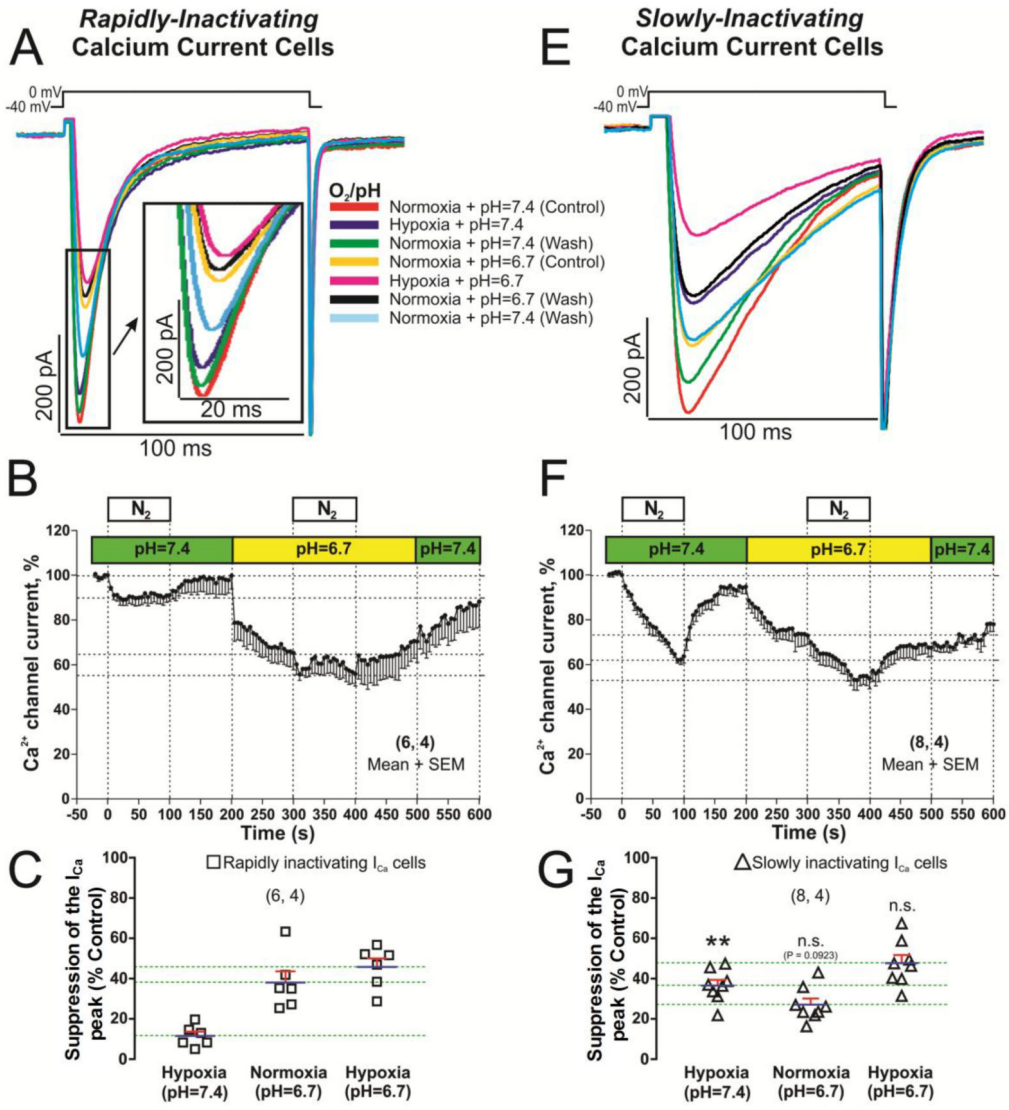

Fig. 7.- L-type Ca^{2+} channel is differentially blocked in hiPSC-CMs with rapidly or slowly inactivating I_{Ca} when the stimulus of acute hypoxia and acidification are combined.

Panels A and E show examples of original traces of rapidly and slowly inactivating I_{Ca} respectively, obtained from two different hiPSC-CMs, activated by depolarization from −40 mV to 0 mV and exposed to the following consecutive treatments: 1) red traces, normoxia and pH (7.4) control condition; 2) dark blue traces, hypoxia and control pH 7.4; 3) green traces, back to the initial control treatment (normoxia and pH 7.4); 4) yellow traces, normoxia and low pH 6.7; 5) pink traces, hypoxia and acidosis combined; 6) black traces, back to normoxia and pH 6.7; 7) light blue traces, washout period to normoxia and pH 7.4. Panels B and F displayed time courses (in hiPSC-CMs with rapidly and slowly inactivating I_{Ca} respectively) of the I_{Ca} suppression by acidosis (pH=6.7 bar) and/or hypoxia (N_2 bar). Panels C and G represents, in dot plots format, the distribution of individual cell values and the average of I_{Ca} blocked (blue lines with SEM represented by red error bars) by hypoxia, acidosis, and both interventions together for both cell types. In the panels B, C, F and G, for

each one of the different data groups, the number of cells (n) and the number of different cultures needed to obtain these data (N) are indicated in parentheses as (n, N). Data were presented as the mean± SEM in this figure. Differences between rapidly and slowly inactivating I_{Ca} cells in hypoxia, acidosis and both stimuli together. $^{**}P < 0.01$; n.s.: not significant; by unpaired two-tailed Student's t-test.

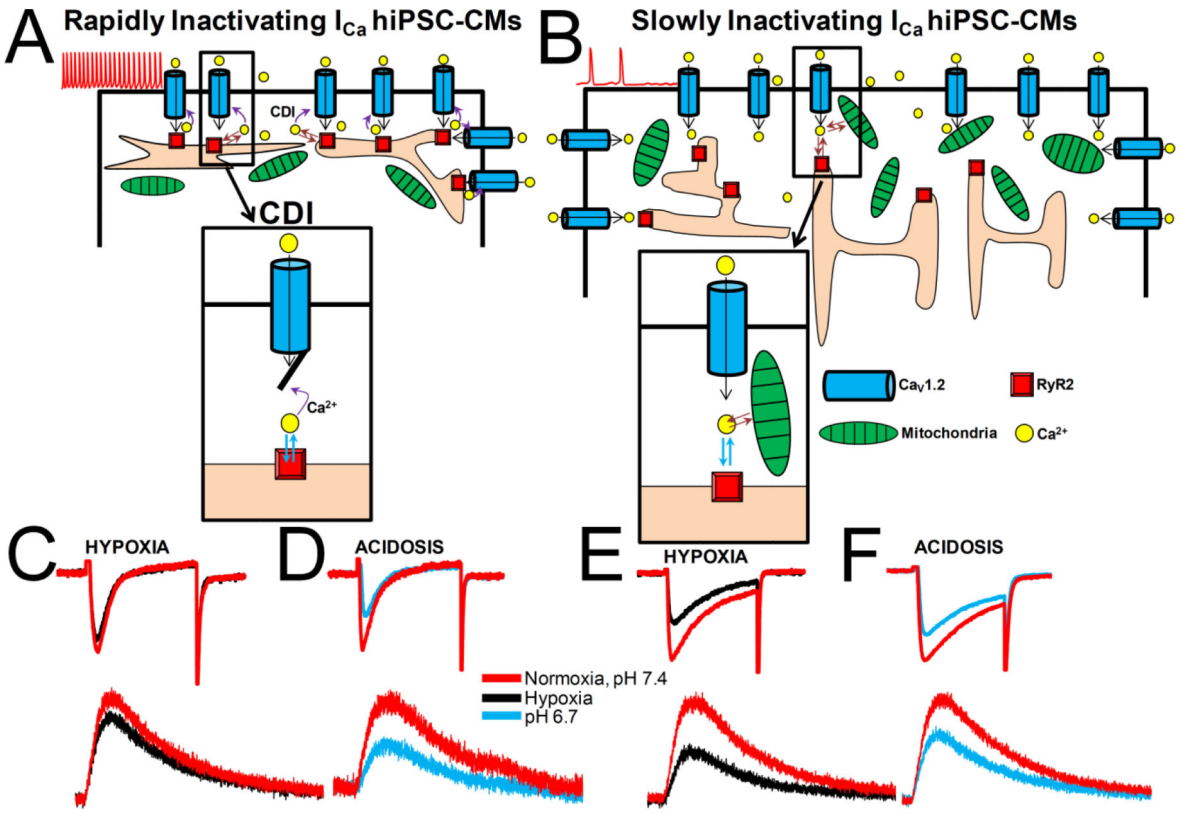

Scheme 1.- Ca^{2+} handling by hiPSC-CMs during acute hypoxia and acidosis.

Two cell-type populations of hiPSC-CMs were identified based on the kinetics of I_{Ca} inactivation during growth in culture. Smaller, 3–4days hiPSC-CMs expressed predominantly rapidly inactivating I_{Ca} (panel A), shorter action potentials, faster spontaneous pacing rates, whereas larger 6–8days hiPSC-CMs expressed mostly slowly inactivating I_{Ca} (panel B) and showed wider APs and slower spontaneous pacing rates ("*Ventricular type APs*"). Acute hypoxia suppress I_{Ca} to a greater degree in slowly inactivating I_{Ca} hiPSC-CMs (~40%, panel E) compared to rapidly inactivating I_{Ca} cells (~15 %, panel C). Suppressive effect of acute acidosis on I_{Ca} (~35%, pH 6.7) was not cell-type dependent (panel D and F). Focal RyR2 Ca^{2+} microdomains were suppressed in a similar range to I_{Ca} inhibition. Acute hypoxia suppresses I_{Ca} in *rapidly inactivating* cell population by a mechanism involving Ca^{2+}-dependent inactivation (insert in panel A), while mitochondrial Ca^{2+} uptake may also contribute to I_{Ca} suppression in *slowly inactivating* cell population (insert in panel B).